

## RESEARCH ACTIVITIES III

### Department of Electronic Structure

#### III-A Synthesis and Characterization of Exotic Molecule Based Nano-Crystals of Metal Acetylides: Toward Carbon Encapsulated Metal Dot Array, Metal Nano-Fibers and Hydrogen Storage

An anhydrous and oxygen-free condition has made us possible to obtain various transition metal-acetylides, where  $M = \text{Fe}, \text{Co}, \text{Ni}$  and so on. These acetylide compounds exhibit high potentiality for magnetic, catalytic, electronic, and gas adsorption functions. In contrast to explosive property of  $M_2C_2$  type acetylides such as  $\text{Ag}_2\text{C}_2$  and  $\text{Cu}_2\text{C}_2$ ,  $\text{CoC}_2$  and  $\text{NiC}_2$  are rather stable in atmospheric condition. Thus, one can make the transition metal acetylides efficiently through the ion exchange reaction of metal chloride with  $\text{CaC}_2$  in dehydrated acetonitrile solution. The  $\text{MC}_2$  type compounds are expected to show  $\text{CaC}_2$  type or  $\text{MgC}_2$  type structure where metal cations and  $\text{C}\equiv\text{C}^{2-}$  are alternatively stacked like a rock salt crystal, although the relative orientation of the anion molecule may depend on the synthetic condition. Annealing or heating above 300 °C induces the reduction of cations by anions,  $\text{C}\equiv\text{C}^{2-}$  (charge neutralization), and resulting in the segregation of metal atoms by locating  $\text{C}_2$  radicals outer and connecting  $\text{C}_2$  bi-radicals as graphite-like or pyrolytic carbon shells. The relatively low segregation temperatures for  $\text{FeC}_2$  and  $\text{NiC}_2$  make it possible to draw metallic dots or wire circuits in  $\text{MC}_2$  thin layers by scanning electron or VUV laser beams. The small size matrix  $\text{MC}_2$  crystals prevent the strong dipole-dipole interaction between the metallic dots, while one can also wash out the matrix salt crystals by acid solution leaving the carbon encapsulated nano-metals on the base plate.

##### III-A-1 Manifestations of Ferromagnetism in $\text{CoC}_2$ by Water Coordination

**NISHIJO, Junichi; OKABE, Chie; NISHI, Nobuyuki; SAWA, Hiroshi<sup>1</sup>**  
(<sup>1</sup>KEK)

Due to the high absorbency of  $\text{CoC}_2$ , water molecules are coordinated to the  $\text{Co}^{2+}$  dication when  $\text{CoC}_2$  is exposed to air or water. XRD pattern of the as-prepared anhydrous  $\text{CoC}_2$ , which is mostly originated from the scattering at the  $\text{Co}^{2+}$  dications, suggests the *fcc*-lattice of  $\text{Co}^{2+}$  with the lattice constants  $a = b = 3.41$  Å and  $c = 4.82$  Å. Judging from the crystal structures of  $\text{CaC}_2$  and  $\text{MgC}_2$ , we expect that the  $\text{Co}^{2+}$  and  $\text{C}_2^{2-}$  ions form NaCl-like alternate stack, where the *fcc* arrangement of the  $\text{Co}^{2+}$  dications indicates the (static) orientation disorder of the  $\text{C}_2^{2-}$  dianions as shown in Figure 1. The cubic structure involving the orientation disorder of  $\text{C}_2^{2-}$  ions is also observed in  $\text{CaC}_2$  at high temperature. Although  $\text{CoC}_2$  is water-stable material unlike  $\text{CaC}_2$  and  $\text{MgC}_2$ , absorbed water changes the crystal structure of  $\text{CoC}_2$  drastically. After air-exposure, the XRD peaks become broad and the positions change as  $\text{Co}^{2+}$  cations form the body-centered-tetragonal sublattice with the lattice constants  $a = b = 3.88$  Å, and  $c = 3.40$  Å. In this phase, the *a*- and *b*-axes are expanded due to the absorbed waters coordinated to the  $\text{Co}^{2+}$ . The orientation of the  $\text{C}_2^{2-}$  dianions is also affected by the lattice expansion and/or steric hindrance of the water, resulting in the structural change from the isotropic disordered orientation (upper case in Figure 1) to anisotropic ordered orientation (lower case in Figure 1). Because the structural change is too drastic to be done in concert,

a  $\text{CoC}_2$  particle is divided into many small domains. Inter-molecular magnetic interaction is sensitive to the arrangement of the molecules. Therefore, it is expected that the magnetism of the hydrous and anhydrous  $\text{CoC}_2$  are largely different. Figure 1 also shows the temperature dependence of the field-cooled magnetic susceptibilities  $\chi$  of  $\text{CoC}_2$  before and after the air-exposure, (a and b, respectively).  $\chi$  of the anhydrous  $\text{CoC}_2$  obeys the Curie-Weiss law in the high temperature range above *ca.* 70 K with Curie constant  $C = 1.1$  emu·K/mol and anti-ferromagnetic (AF) Weiss temperature  $\Theta = -10$  K, the former of which is obviously larger than the value of  $\text{Co}^{2+}$  cation ( $C = 0.375$ ), suggesting the short-range strong ferromagnetic (FM) interaction. Although  $\chi$  of the hydrous  $\text{CoC}_2$  also obeys the Curie-Weiss law above 100 K,  $C = 1.5$  emu·K/mol is significantly larger than that of anhydrous  $\text{CoC}_2$  suggesting the expansion of the FM domain, while AF  $\Theta = -3$  K indicates the weakening of the AF interaction between FM domains. The difference of the magnetism between hydrous and anhydrous  $\text{CoC}_2$  is evidently caused by the water-induced structural changes; that is, the orientation ordering of  $\text{C}_2^{2-}$  and the expansion of the inter-chain distance. Judging from the fact that the interaction is weakened by lengthening the inter-molecular distance, it is concluded that the AF and FM interactions are attributed to the inter- and intra-chain interaction. In hydrous phase, where the FM interactions are connected each other and form the FM chain elongated parallel to the *c*-axis, resulting in the large FM domains.

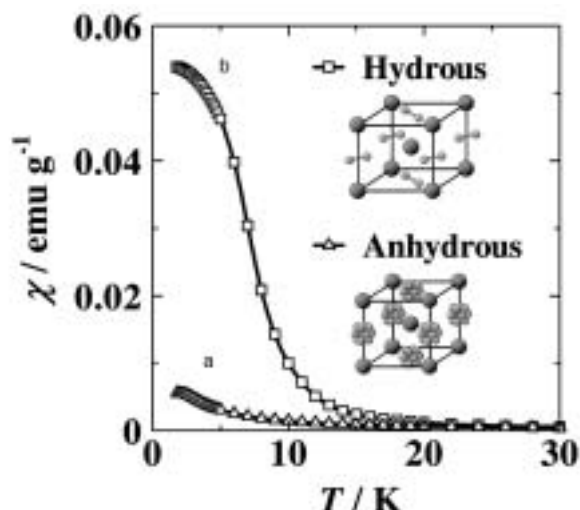


**Figure 1.** Temperature dependence of the field-cooled (10 Oe) magnetic susceptibilities  $\chi$  of  $\text{CoC}_2$  before and after the air-exposure. (a and b, respectively). Inserted are the structures that reproduce the XRD patterns of hydrous and anhydrous  $\text{CoC}_2$  nano-crystals.

### III-A-2 Molecule-Based Room Temperature Magnet: $(\text{CoC}_2)_2(\text{H}_2\text{O})$ Nano-Rods

KOSUGI, Kentaroh; NISHIJO, Junichi; OKABE, Chie; BUSHIRI, Junaid M.; NISHI, Nobuyuki

As revealed in the previous study,  $\text{CoC}_2$  crystals become ferromagnetic with coordinating water molecules to  $\text{Co}^{2+}$  ions. Elongation of the  $\text{Co}^{2+}$ - $\text{Co}^{2+}$  distance makes the four-center interaction positive with the  $\text{C}_2^{2-}$  molecular axis perpendicular to the  $\text{Co}$ - $\text{Co}$  axis.  $(\text{CoC}_2)_2(\text{H}_2\text{O})$  was synthesized from acetonitrile solution of  $\text{CoCl}_2$  and suspended  $\text{CaC}_2$  powder at 100 °C. The black product was washed by methanol with 5% of water. Figure 1 shows TEM images of the nano-rods. Figure 1-a indicates the presence of small particles with several nm radii in addition to the rod-like particles. Expanded in Figure 1-b is the lattice pattern of a rod exhibiting the long distances of the lattice stripes and wavy or somewhat disordered orientation of the atoms in the lattice sites. This kind of disorder is hardly seen in metal oxides or metallic particles with similar sizes. This is probably due to gradual hydration after the salt type crystals were formed, and thought to be characteristic of hydrophilic acetylide compounds. Figure 1-c shows the magnetic hysteresis curves of the particles at 300 K and 1.8 K. As seen from the curves, cohesive forces are as large as 780 Oe at 1.8 K and 650 Oe at 300 K. The magnetic saturation curve at 1.8 K suggests that the small spherical particles are superparamagnetic at 300K and only the rod-type crystals behave as room temperature magnets.

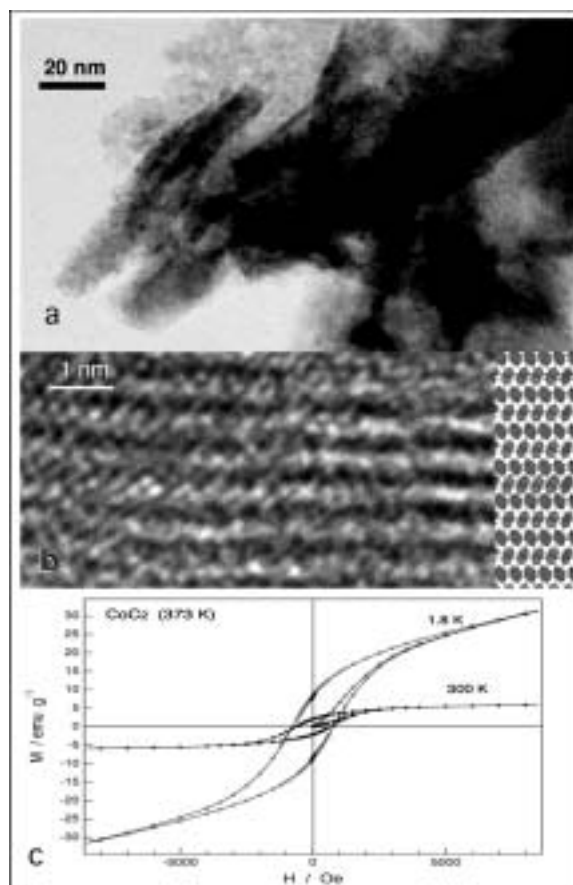


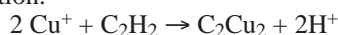
**Figure 1.** a: Transmission Electron Microscope image of the  $(\text{CoC}_2)_2(\text{H}_2\text{O})$  nano-rods that coexist with small spherical particles with several nm radii. b: Expanded view of a lattice image of a nano-rod. c: Magnetic hysteresis curves of  $\text{CoC}_2$  synthesized at 100 °C.

### III-A-3 Self-Assembled Nano-Wire Formation of Copper Acetylide ( $\text{C}_2\text{Cu}_2$ )

JUDAI, Ken; NISHIJO, Junichi; OKABE, Chie; NISHI, Nobuyuki

Copper acetylide ( $\text{Cu}-\text{C}\equiv\text{C}-\text{Cu}$ ) was synthesized firstly for a long time ago, however, because of its explosive nature, the revealed properties are limited. From the view point of nano-science, the extreme small amount of explosive compound cannot achieve critical point of explosion, and is regarded as good candidate for source of copper or carbon in the dimension of nano-scale. The other side, recent progress of electron microscopy makes it possible to uncover geometric structure of various compounds in atomic scale. We have examined synthesized copper acetylide by transmission electron microscopy (TEM), and its self-assembled nano-rod shape was discovered.

The copper acetylide was synthesized by the following recipe. First, 1 g of copper chloride (I),  $\text{CuCl}$ , was dissolved into 100 ml of 6% ammonia water. After 30 minutes of Ar gas bubbling in order to remove dissolved oxygen molecules, acetylene ( $\text{C}_2\text{H}_2$ ) gas was bubbled in the solution.



The color of the solution turned from blue (copper

amine complex) into dark brown, and the product of  $C_2Cu_2$  was precipitated. After 30 minutes reaction, the product was filtered and washed by water and methanol. Since this product contained excess solvent molecules, the estimation of the reaction yield was difficult. Very roughly, 50 ~ 100% of yield was guessed. For the measurement of TEM, small amount of the product was grinded and suspended in methanol. The methanol suspension was dropped onto a micro grid. After dry up, that grid was used as a specimen for TEM observation.

Figure 1 displays the TEM images of copper acetylide. Even if the copper acetylide synthesized in water solution was measured directly by TEM, nano-wires shaped with 5–20 nm of diameter and 200–800 nm in length were observed. This means that  $C_2Cu_2$  in water solution is self-assembled into nano-sized rod structure. Due to the minimization of the electronic circuit on computer, production of nano-wires is one of the hottest topics in nano-technology. The various methods have been suggested for production ways of nano-wires, for example, nano-single crystal wire growth on nano-sized catalysis, deposition of metal on a template with nano-holes, and so on. The self-assembled method for nano-wire production is easily applied to mass-production and low-cost compared to the other method. The way of synthesis for nano-wire  $C_2Cu_2$  is so simple that this is regarded as a remarkable way. Its crystal structure, aggregation mechanism, and physical properties (conductivity and so on) are still unclear in the present stage. In our group the theoretical calculation and various analysis techniques are in progress to reveal nature of copper acetylide nano-wire in detail.

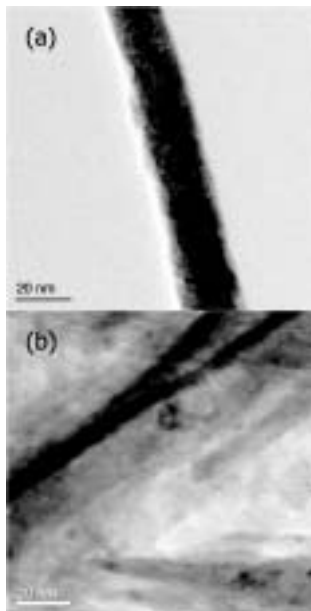


**Figure 1.** (a): Transmission Electron Microscope (TEM) image of copper acetylide ( $C_2Cu_2$ ). 20 nm of rod diameter is one of the thickest wires. (b): Typical TEM image of copper acetylide ( $C_2Cu_2$ ). The bundle of nano-wires with 5 nm of diameter was observed.

### III-A-4 Formation of Air Stable Carbon-Skinned Iron Nanocrystals from $FeC_2$

KOSUGI, Kentaroh; BUSHIRI, Junaid M.; NISHI, Nobuyuki

[*Appl. Phys. Lett.* **84**, 1753–1755 (2004)]

Charge neutralization reaction in ionic salt of  $Fe^{2+}C_2^{2-}$  is found to produce carbon-skinned Fe nanocrystals.  $FeC_2$  is formed as an intermediate product in the reaction of  $FeCl_2$  solved in acetonitrile with  $CaC_2$  fine powder and also able to be isolated as black nanocrystals. Heating of  $FeC_2$  at temperature higher than 250 °C induces segregation of metallic iron. The segregated carbons grow as graphitic sheets parallel to the growing Fe lattice plane. This direct bonding is due to an accidental matching of the Fe–Fe distance (2.866 Å) with that of the  $C_1$ – $C_4$  distance (2.842 Å) of the hexagonal rings in graphite. The X-ray diffraction pattern indicates that the particles are composed of  $\alpha$ -Fe and graphitic carbon. The thickness of the skin is almost constant as thick as 3.5 nm independent of the body size. The particles with an average size of 30 nm exhibit temperature dependence of the magnetic cohesive force as function of  $T^{-0.275}$ .

## III-B States of Neutral and Ionic Molecular Associates in Solutions

States of molecular associates particularly in aqueous solutions are of great importance in understanding the role of molecules in living organisms. We found that any ideally mixed state cannot be seen in protic-protic mixtures such as water-alcohol, water-acetic acid, and alcohol-acetic acid systems on the molecular level at solute molar fractions ( $\chi_A$ ) higher than 0.001. In such a system, solute-solute association is highly favored resulting in microscopic phase separation. In this year, we studied the aqueous mixture of hexafluoro-2-propanol (HFIP), and have shown that that structural transition of solvent clusters takes place at  $x_{\text{HFIP}} \sim 0.1$  from the tetrahedral-like hydrogen bonded network of water at  $x_{\text{HFIP}} \leq \sim 0.1$  to the structure of near HFIP gradually formed with increasing HFIP concentration in the range of  $x_{\text{HFIP}} \geq 0.15$ .

### III-B-1 Structure and Dynamics of Hexafluoroisopropanol-Water Mixtures by X-Ray Diffraction, Small-Angle Neutron Scattering, NMR Spectroscopy, and Mass Spectrometry

YOSHIDA, Koji<sup>1</sup>; YAMAGUCHI, Toshio<sup>1</sup>;  
ADACHI, Tomohiro<sup>2</sup>; OTOMO, Toshiya<sup>2</sup>;  
MATSUO, Daisuke<sup>3</sup>; TAKAMUKU, Toshiyuki<sup>3</sup>;  
NISHI, Nobuyuki  
(<sup>1</sup>Fukuoka Univ.; <sup>2</sup>KEK; <sup>3</sup>Saga Univ.)

[*J. Chem. Phys.* **119**, 6132–6142 (2003)]

The structure and dynamic properties of aqueous mixtures of 1,1,1,3,3,3-hexafluoro-2-propanol (HFIP) have been investigated over the whole range of HFIP mole fraction ( $x_{\text{HFIP}}$ ) by large-angle x-ray scattering (LAXS), small-angle neutron scattering (SANS), <sup>19</sup>F-, <sup>13</sup>C-, and <sup>17</sup>O-NMR chemical shifts, <sup>17</sup>O-NMR relaxation, and mass spectrometry. The LAXS data have shown that structural transition of solvent clusters takes place at  $x_{\text{HFIP}} \sim 0.1$  from the tetrahedral-like hydrogen bonded network of water at  $x_{\text{HFIP}} \leq \sim 0.1$  to the structure of near HFIP gradually formed with increasing HFIP

concentration in the range of  $x_{\text{HFIP}} \geq 0.15$ . The Ornstein-Zernike plots of the SANS data have revealed a mesoscopic structural feature that the concentration fluctuations become largest at  $x_{\text{HFIP}} \sim 0.06$  with a correlation length of  $\sim 9$  Å, *i.e.*, maximum in clustering and microheterogeneities. The <sup>19</sup>F and <sup>13</sup>C chemical shifts of both CF<sub>3</sub> and CH groups of HFIP against  $x_{\text{HFIP}}$  have shown an inflection point at  $x_{\text{HFIP}} \sim 0.08$ , implying that the environment of HFIP molecules changes due to the structural transition of HFIP clusters. The <sup>17</sup>O relaxation data of water have shown that the rotational motion of water molecules is retarded rapidly upon addition of HFIP into water up to  $x_{\text{HFIP}} \sim 0.1$ , moderately in the range of  $\sim 0.1 < x_{\text{HFIP}} \leq 0.3$ , and almost constant at  $x_{\text{HFIP}} \geq 0.3$ , reflecting the structural change in the solvent clusters at  $x_{\text{HFIP}} \sim 0.1$ . The mass spectra of cluster fragments generated in vacuum from HFIP-water mixtures have shown that the predominant clusters are A<sub>1</sub>W<sub>n</sub> ( $n < 12$ , A = HFIP, W = water) and water clusters W<sub>n</sub> ( $n = 5-8$ ) at  $x_{\text{HFIP}} = 0.09$  and 0.20 and only HFIP oligomers in a water-rich region  $x_{\text{HFIP}} = 0.005 \sim 0.01$ . From all the information obtained in the present study, the models are proposed for the aggregation of HFIP and water molecules in HFIP-water mixtures.

## III-C Ultrafast Dynamics and Scanning Tunneling Microscopy

For the study of molecules on metallic or crystalline surface, very low temperature Scanning Tunneling Microscope (LT STM) system are now in use for collaboration with users in universities. Ultrafast laser systems with pico and femtosecond time resolutions are also available.

### III-C-1 Orientation of Adsorbed Nitrous Oxide on Palladium(110) by STM

MATSUSHIMA, Tatsuo<sup>1</sup>; RZEZNICKA, Izabela<sup>1</sup>;  
WATANABE, Kazuo<sup>2</sup>; INOKUCHI, Yoshiya<sup>2</sup>;  
NISHI, Nobuyuki  
(<sup>1</sup>Hokkaido Univ.; <sup>2</sup>Univ. Tokyo)

Adsorbed N<sub>2</sub>O on Pd(110) was confirmed to be oriented along the [001] direction at around 8 K by using a low temperature scanning-tunneling microscope, confirming the prediction from angular distributions of

desorbing product N<sub>2</sub> in thermal N<sub>2</sub>O decomposition and through structure analysis of adsorbed N<sub>2</sub>O by density functional theory with generalized gradient approximations. Figure 1 shows a STM image of N<sub>2</sub>O-covered Pd(110) at 8 K. Furthermore, the formation of small clusters extended along the [110] direction was first found at low temperatures. These measurements support the reaction mechanism through the N<sub>2</sub>O intermediate in catalytic NO<sub>x</sub> decomposition.

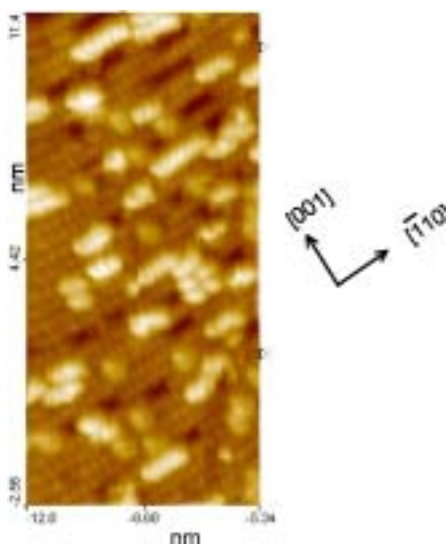


**Figure 1.** A STM image of  $\text{N}_2\text{O}$ -covered Pd(110) at 8 K.  $\text{N}_2\text{O}$  was dosed at 90–80 K.

### III-C-2 Observation of Ultrafast Dynamics of Jet-Cooled *N*-Salicylideneaniline by Femtosecond Time-Resolved REMPI Spectroscopy

OKABE, Chie; NAKABAYASHI, Takakazu<sup>1</sup>; INOKUCHI, Yoshiya<sup>2</sup>; SEKIYA, Hiroshi<sup>3</sup>; NISHI, Nobuyuki

(<sup>1</sup>Hokkaido Univ.; <sup>2</sup>Univ. Tokyo; <sup>3</sup>Kyushu Univ.)

[*J. Chem. Phys.* **121**, 9436–9422 (2004)]

*N*-salicylideneaniline (SA) is well-known photochromic aromatic anil. The excited-state intramolecular proton transfer (ESIPT) followed by photoexcitation of the enol form to its first  $^1(\pi, \pi^*)$  state produces the  $^1(\pi, \pi^*)$  state of the *cis*-keto form, leading to a meta-stable *trans*-keto form as the final photoproducts. To investigate ultrafast processes in photoexcited SA, we have applied the femtosecond time-resolved resonance-enhanced multiphoton ionization (REMPI) spectroscopy under the isolated conditions. The decay profile of SA excited at 320 nm is well reproduced by a convolution of the response function with a bi-exponential decay, giving time constants of  $\tau_1 < 300$  fs and  $\tau_2 = 3.3$  ps. The decay profile of SA measured by varying the pump wavelength from 360 to 373 nm is well fitted using a tri-exponential decay function with time constants of  $\tau_1 < 300$  fs,  $\tau_3 = 1.5$  ps, and  $\tau_4 > 100$  ps. The difference is attributable to the difference in the ionization efficiency for the enol and keto forms. A very fast decay component ( $\tau_1 < 300$  fs) is assigned to a decay of the  $^1(\pi, \pi^*)$  state of the enol form. A component  $\tau_3 = 1.5$  ps arises from the *cis*-keto form produced *via* the excited-state intramolecular proton transfer (ESIPT) reaction, because the probe wavelength at  $\sim 400$  nm is in resonance with the  $S_n-S_1$  transition of the *cis*-keto form. A component  $\tau_2 = 3.3$  ps is attributed to the decay of an excited state of the enol form. The ion signals *via* the  $^1(n, \pi^*)$  state of the enol form as well as the proton-transferred *cis*-keto form emerge within a few hundred femtoseconds after photo-excitation to the first  $^1(\pi, \pi^*)$

state of the enol form. This state must be populated *via* the  $^1(n, \pi^*)$  state of the enol form, suggesting that an ultrafast non-radiative process occurs in addition to the ESIPT reaction.

Figure 1 shows the deactivation processes following the photoexcitation of the enol form on the basis of the results of the femtosecond time-resolved REMPI measurement together with the theoretical studies. Two ultrafast processes, the ESIPT reaction and an internal conversion (IC) to the  $^1(n, \pi^*)$  state, occur on a time scale less than a few hundred femtoseconds from the  $^1(\pi, \pi^*)$  state of the enol form. The decay time of the  $^1(\pi, \pi^*)$  state of the *cis*-keto form largely changes when the enol form is excited at between 370 and 365 nm. The remarkable change in the decay time is reasonably explained by the existence of a threshold for the ultrafast non-radiative process from the  $^1(\pi, \pi^*)$  state of the *cis*-keto form. The opening of an efficient non-radiative channel; an IC from  $^1(\pi, \pi^*)$  to  $^1(n, \pi^*)$  of the *cis*-keto form promotes the production of the *trans*-keto form as the final photochromic products. The two IC processes provide opposite effect on the quantum yield of photochromic products: IC in the enol form may substantially reduce the quantum yield, but IC in the *cis*-keto form increases it.

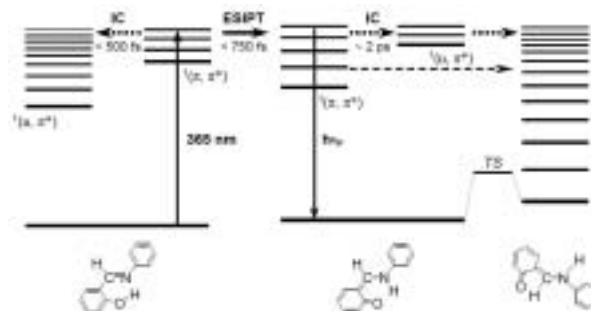


**Figure 1.** Photoexcited processes of SA drawn on the basis of the femtosecond time-resolved REMPI spectroscopy in gas phase. Two ultrafast processes ESIPT and IC occur by photoexcitation of a high vibronic state of the enol form. When the pump wavelength is shorter than  $\sim 365$  nm, an IC occurs from the  $^1(\pi, \pi^*)$  to the  $^1(n, \pi^*)$  state of the proton-transferred *cis*-keto form in addition to the radiative ( $h\nu_f$ ) and non-radiative decay to the  $S_0$  state. The IC efficiently produces the *trans*-keto form as the final photochromic products. The *trans*-keto form may be produced as a minor channel when the enol form is excited at wavelength longer than 370 nm. *TS* indicates a transition state.

### III-C-3 Picosecond Time-Resolved Stokes and Anti-Stokes Raman Studies on the Photochromic Reactions of Diarylethene Derivatives

OKABE, Chie; NAKABAYASHI, Takakazu<sup>1</sup>; NISHI, Nobuyuki; FUKAMINATO, Tuyoshi<sup>2</sup>; KAWAI, Tsuyoshi<sup>2</sup>; IRIE, Masahiro<sup>2</sup>; SEKIYA, Hiroshi<sup>2</sup>

(<sup>1</sup>Hokkaido Univ.; <sup>2</sup>Kyushu Univ.)

[*J. Phys. Chem. A* **107**, 5384–5390 (2003)]

The cyclization and cycloreversion reactions of diarylethene derivatives have been studied with picosecond time-resolved Stokes and anti-Stokes Raman spectroscopies. The cyclization reaction of 1,2-bis(2,5-dimethyl-3-thienyl)perfluorocyclopentene (DMTF) is found to occur within 4 ps to produce the vibrationally excited closed forms in the ground electronic ( $S_0$ ) state. The time constant of the vibrational relaxation toward a thermal equilibrium with solvent molecules is estimated to be about 10 ps. The cycloreversion reaction of 1,2-bis(3,4-dimethyl-5-phenyl-2-thienyl)perfluorocyclopentene (DMPTF) also generates the vibrationally excited open forms in the  $S_0$  state within 4 ps, which

decay on a picosecond time scale. The picosecond time-resolved anti-Stokes Raman spectra of DMPTF show two vibrational bands assignable to the C=C stretching modes of the cyclopentene and thiophene moieties of the generated open forms. The Raman intensity arising from the cyclopentene moiety relative to that from the thiophene moiety becomes smaller with the delay time, indicating that part of the excess energy generated *via* the cycloreversion reaction is localized on the C=C stretching mode of the cyclopentene moiety. This result suggests that the C=C stretching mode of the cyclopentene moiety is one of the promoting or the accepting modes in the cycloreversion reaction.

## III-D Spectroscopic and Dynamical Studies of Molecular Cluster Ions

Electron deficiency of molecular cluster cations can attract electron rich groups or atoms exhibiting charge transfer or charge resonance interaction in the clusters. This causes dynamical structural change such as proton transfer or ion-core switching in hot cluster ions or clusters in solution.

### III-D-1 Structures of $[\text{Mg}\cdot(\text{H}_2\text{O})_{1,2}]^+$ and $[\text{Al}\cdot(\text{H}_2\text{O})_{1,2}]^+$ Ions Studied by Infrared Photodissociation Spectroscopy: Evidence of $[\text{HO}-\text{Al}-\text{H}]^+$ Ion Core Structure in $[\text{Al}\cdot(\text{H}_2\text{O})_2]^+$

INOKUCHI, Yoshiya<sup>1</sup>; OHSHIMO, Keijiro<sup>2</sup>; MISAIZU, Fuminori<sup>3</sup>; NISHI, Nobuyuki  
(<sup>1</sup>IMS and Univ. Tokyo; <sup>2</sup>RIKEN; <sup>3</sup>Tohoku Univ.)

[*Chem. Phys. Lett.* **390**, 140–144 (2004)]

Infrared spectra of  $[\text{Mg}\cdot(\text{H}_2\text{O})_{1,2}]^+$  and  $[\text{Al}\cdot(\text{H}_2\text{O})_{1,2}]^+$  are measured in the OH stretching region (3200–3800  $\text{cm}^{-1}$ ). The spectra show the symmetric and asymmetric OH stretching bands of water molecules that are directly bound to the metal ions through metal-oxygen intermolecular bonds. In addition to these bands, the  $[\text{Al}\cdot(\text{H}_2\text{O})_2]^+$  ion has another band at 3714  $\text{cm}^{-1}$ . This band is assigned to the free OH stretching vibration of the  $[\text{HO}-\text{Al}-\text{H}]^+$  ion; the aluminum ion is inserted into the O–H bond of one water molecule in  $[\text{Al}\cdot(\text{H}_2\text{O})_2]^+$ .

### III-D-2 Infrared Photodissociation Spectroscopy of $[\text{Mg}\cdot(\text{H}_2\text{O})_{1-4}]^+$ and $[\text{Mg}\cdot(\text{H}_2\text{O})_{1-4}\cdot\text{Ar}]^+$

INOKUCHI, Yoshiya; OHSHIMO, Keijiro; MISAIZU, Fuminori<sup>1</sup>; NISHI, Nobuyuki  
(<sup>1</sup>Tohoku Univ.)

[*J. Phys. Chem. A* **108**, 5034 (2004)]

Infrared photodissociation spectra of  $[\text{Mg}\cdot(\text{H}_2\text{O})_{1-4}]^+$  and  $[\text{Mg}\cdot(\text{H}_2\text{O})_{1-4}\cdot\text{Ar}]^+$  are measured in the 3000–3800  $\text{cm}^{-1}$  region. For  $[\text{Mg}\cdot(\text{H}_2\text{O})_{1-4}]^+$ , cluster geometries are optimized and vibrational frequencies

are evaluated by density functional theory calculation. We determine cluster structures of  $[\text{Mg}\cdot(\text{H}_2\text{O})_{1-4}]^+$  by comparison of the infrared photodissociation spectra with infrared spectra calculated for optimized structures of  $[\text{Mg}\cdot(\text{H}_2\text{O})_{1-4}]^+$ . In the  $[\text{Mg}\cdot(\text{H}_2\text{O})_{1-3}]^+$  ions, all the water molecules are directly bonded to the  $\text{Mg}^+$  ion. The infrared photodissociation spectra of  $[\text{Mg}\cdot(\text{H}_2\text{O})_4]^+$  and  $[\text{Mg}\cdot(\text{H}_2\text{O})_4\cdot\text{Ar}]^+$  show bands due to hydrogen-bonded OH stretching vibrations in the 3000–3450  $\text{cm}^{-1}$  region. In the  $[\text{Mg}\cdot(\text{H}_2\text{O})_4]^+$  ion, three water molecules are attached to the  $\text{Mg}^+$  ion, forming the first solvation shell; the fourth molecule is bonded to the first solvation shell. As a result, the most stable isomer of  $[\text{Mg}\cdot(\text{H}_2\text{O})_4]^+$  has a six-membered ring composed of the  $\text{Mg}^+$  ion, two of the three water molecules in the first solvation shell, and a termination water molecule.

### III-E Spectroscopy and Dynamics of Vibrationally Excited Molecules and Clusters

This research group is studying structure and dynamics of molecules and clusters by two-color double resonance spectroscopy. New spectroscopic methods will also be developed to observe the higher vibrational state under collision-free condition.

A molecular cluster is a microscopic system of solution and/or crystal, and is thought to provide detailed information on relaxation and reaction dynamics in condensed phase. However the previous studies are concentrated to stable clusters which has no reaction pathway after photo-excitation. Consequently, spectroscopic information which concerns the reaction mechanism has not been obtained sufficiently. In this research project started from 2000, we will apply various laser spectroscopies to the reactive clusters to reveal detailed mechanism of intracuster reaction.

For the study of the ground state, the structure of the cluster can be determined by the combination of the IR dip spectroscopy and *ab initio* MO calculations.<sup>1)</sup> The IR dip spectroscopy is a kind of IR-UV double resonance spectroscopy which provides the spectrum which corresponds to the infrared absorption spectrum of the cluster (see Figure 1). A tunable IR laser is introduced to the clusters and is scanned its frequency over the fundamental vibrational region (typically 2400 ~ 4000  $\text{cm}^{-1}$ ). Then a tunable UV laser, of which the frequency is fixed to the  $S_1$  origin of a specific cluster, is introduced and resonant enhanced multiphoton ionization signal *via*  $S_1$  is monitored. When the IR laser is resonant to a vibrational level of the cluster, the ion signal decreases much because of loss of the population in the vibrational ground state. Thus, the IR absorption spectrum of the cluster can be measured by this depletion spectroscopy. The same spectrum can be obtained when the fluorescence intensity from  $S_1$  is monitored instead of the ion current.

The IR spectrum in the excited state  $S_1$  can also be measured by the depletion spectroscopy, when the UV laser is introduced before the IR laser (the UV-IR fluorescence dip spectroscopy; see Figure 2). The molecule is excited to  $S_1$  by the UV laser, and the fluorescence intensity is monitored as well as the IR dip spectroscopy for  $S_0$ . Then the  $S_1$  molecules are further excited to the vibrationally excited level in  $S_1$  by the IR laser. In general, the fluorescence quantum yield decreases in the higher vibronic level. Thus, the total fluorescence intensity decreases when the IR laser frequency is resonant to the vibrational level in  $S_1$ .

Similarly, the IR spectrum of the ionic cluster can be measured by the depletion spectroscopy (mass-selected ion dip spectroscopy; see Figure 3). The ionic cluster can be prepared by the multiphoton ionization *via*  $S_1$ , and the ion current due to the cation cluster of the specific size can be measured through a mass-filter. When the ionic cluster is vibrationally excited by the IR laser, the cluster is dissociated by the vibrational predissociation. Therefore, the IR transition can be measured by the decrease of the parent cluster. The same spectrum can be obtained by monitoring the enhancement of fragments (mass-selected multiphoton dissociation spectroscopy). In addition to these "dip" spectroscopies, the nonresonant ionization detected IR spectroscopy<sup>2)</sup> and the PFI-ZEKE photoelectron spectroscopy<sup>3)</sup> are also important tool to obtain the spectral information in the cation and the overtone states. Based on these spectroscopic techniques, we have measured the IR spectra of solvated clusters,<sup>4)</sup> such as phenol/ammonia,<sup>5)</sup> naphthol/alcohol,<sup>6)</sup> carbazole/water<sup>7)</sup> and 7-azaindole dimers,<sup>8)</sup> and have discussed the relation among geometrical structure, electronic state and intracuster reactions.

From 2001, we have been developing the new ultrafast time-resolved IR spectroscopy for the reactive clusters. The pico second time-resolved vibrational spectroscopy is one of the ideal way to reveal the reaction mechanism directly. Here, we will demonstrate its usefulness by applying the hydrogen transfer reaction in photoexcited PhOH-

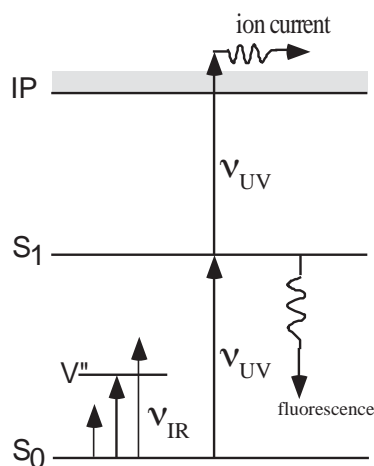


**Figure 1.** Principle of the IR Dip Spectroscopy. The IR transition in the ground state cluster can be measured.

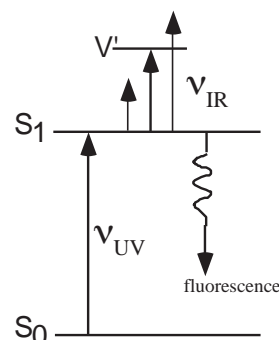


**Figure 2.** Principle of the UV-IR Fluorescence Dip Spectroscopy. The IR transition of the cluster in the  $S_1$  state can be obtained.

( $\text{NH}_3$ ) $_n$  cluster.<sup>9)</sup> Figure 4 shows the principle of the picosecond time-resolved UV-IR-UV ion dip spectroscopy. The reactive cluster ( $\text{PhOH}-(\text{NH}_3)_n$  in present case) is excited to  $S_1$  by a picosecond UV laser  $\nu_{\text{UV}}$  and the photochemical reaction (hydrogen transfer) is triggered. The final reaction product, *i. e.* ( $\text{NH}_3$ ) $_{n-1}\text{NH}_4$ , is ionized by a nanosecond UV laser  $\nu_{\text{ION}}$  which is irradiated after 100 ns from  $\nu_{\text{UV}}$  and the population of the reaction product is monitored as a mass peak of ( $\text{NH}_3$ ) $_{n-1}\text{NH}_4^+$ . A picosecond tunable IR laser  $\nu_{\text{IR}}$  is irradiated after  $t$  ps from  $\nu_{\text{UV}}$  and is scanned over vibrational region. If  $\nu_{\text{IR}}$  is resonant to vibrational levels of the transient species, the population of the final reaction product decreases due to the vibrational predissociation of the transient species. Therefore, the vibrational transitions of the transient species at  $t$  ps can be observed as decrease of ion current of the final reaction product.

Time resolved UV-IR-UV ion dip spectra of phenol-( $\text{NH}_3$ ) $_3$  are shown in Figure 5. The numbers in the left hand sides of each spectrum indicate the delay time from  $\nu_{\text{UV}}$  to  $\nu_{\text{IR}}$ . Here the spectrum at  $-20$  ns corresponds to the IR spectrum of  $\text{PhOH}-(\text{NH}_3)_3$  in  $S_0$ , in which the sharp bands around  $3400\text{ cm}^{-1}$ , the broad bands at  $\sim 3200\text{ cm}^{-1}$  and the very broad background are assigned to the degenerated antisymmetric stretch vibration  $\nu_3$  in  $\text{NH}_3$ , the totally symmetric stretch vibration  $\nu_1$  in  $\text{NH}_3$  and the OH stretch vibration  $\nu_{\text{OH}}$  in phenol, respectively. The spectrum at  $+180$  ns shows the vibrational transitions of the final reaction product *via*  $S_1$ , *i. e.* ( $\text{NH}_3$ ) $_2\text{NH}_4$ , and 1) two intense bands at  $3180\text{ cm}^{-1}$  and  $3250\text{ cm}^{-1}$  and 2) a broad band at  $2700 \sim 3100\text{ cm}^{-1}$  which have been assigned to

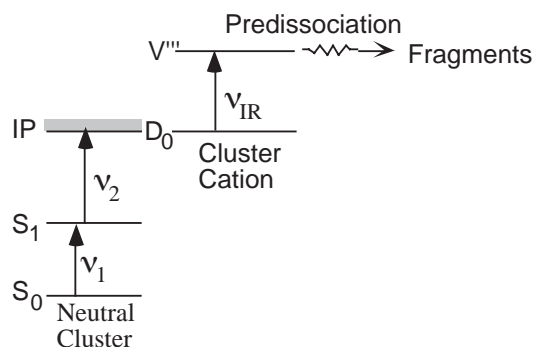


**Figure 3.** Principle of the mass-selected IR Ion Dip Spectroscopy. The IR transition of the cluster cation can be measured by the depletion of the parent cluster cation. The same spectrum can be measure by monitoring the enhancement of the fragments produced by the IR predissociation.

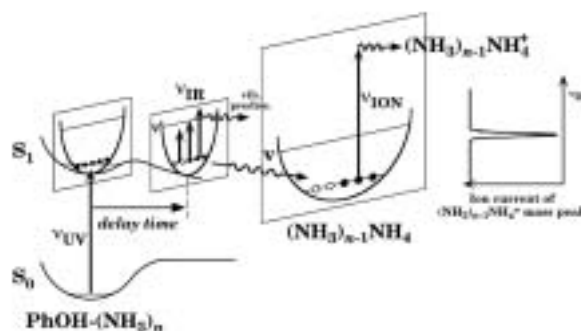


**Figure 4.** Principle of picosecond time-resolved UV-IR-UV ion dip spectroscopy. Potential curves of  $S_0$  and  $S_1$  are schematically drawn along O–H stretch coordinate. Potential curves in different sections on the  $S_1$  O–H stretch coordinate are drawn along arbitrary N–H stretch coordinates.

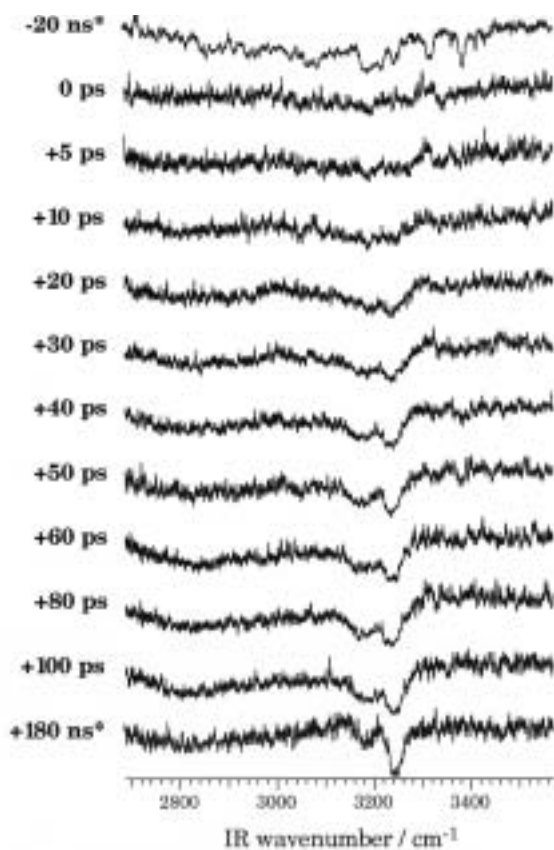


**Figure 5.** Picosecond time-resolved UV-IR-UV ion dip spectra of the transient species from the electronically excited  $\text{PhOH}-(\text{NH}_3)_3$  which was observed by fixing  $\nu_{\text{UV}}$  to the low vibronic band in the  $S_1$  state of  $\text{PhOH}-(\text{NH}_3)_3$  ( $281.49\text{ nm}$ ) and monitoring ( $\text{NH}_3$ ) $_2\text{NH}_4^+$  due to  $\nu_{\text{ION}}$  ( $355\text{ nm}$ ). Times indicated at the left side of each spectrum mean the delay times between  $\nu_{\text{UV}}$  and  $\nu_{\text{IR}}$ . The spectra whose delay times are  $-20\text{ ns}$  and  $+180\text{ ns}$  (indicated by \*) are obtained by nanosecond laser system, which have been reported in the previous paper.<sup>5)</sup>

vibrational transitions concerned with  $\text{NH}_4$ .

One can see that the vibrational bands rise with increasing delay time. The spectral feature at +100 ps is already similar to that of the final reaction product (+180 ns). Here, the intense band at  $3250\text{ cm}^{-1}$  rises slower than the band at  $3180\text{ cm}^{-1}$ . The relative intensities of the two bands become comparable at 40 ps, thereafter, the higher band at  $3250\text{ cm}^{-1}$  clearly grows further. Thus, the rising time constant of the band at  $3250\text{ cm}^{-1}$  is apparently different from that of the  $3180\text{ cm}^{-1}$ -band. This remarkable difference between the two intense bands suggests that each vibrational transition is derived from different species. The existence of two transient species are naturally interpreted by considering the isomers of  $(\text{NH}_3)_2\text{NH}_4$ ; the most stable  $\text{NH}_3\text{-NH}_4\text{-NH}_3$  and the meta-stable  $\text{NH}_4\text{-NH}_3\text{-NH}_3$ . The co-existence of isomers is strongly supported by *ab initio* calculations.

As described above, we have successfully measured the picosecond time resolved IR spectra of the transient species for the ESHT of  $\text{PhOH-(NH}_3)_3$  for the first time. It proves that the picosecond UV-IR-UV ion dip spectroscopy is a powerful tool to explore the dynamics of the intracuster reaction.

## References

- 1) R. Yoshino *et al.*, *J. Phys. Chem. A* **102**, 6227 (1998).
- 2) T. Omi *et al.*, *Chem. Phys. Lett.* **252**, 287 (1996); S. Ishiuchi *et al.*, *Chem. Phys. Lett.* **283**, 243 (1998).
- 3) K. Takazawa *et al.*, *Chem. Phys. Lett.* **189**, 592 (1992); K. Müller-Dethlefs *et al.*, *Z. Naturforsch. Teil A* **39**, 1089 (1984); K. Müller-Dethlefs and M. C. R. Cockett, "Zero Kinetic Energy (ZEKE) Photoelectron Spectroscopy," Chapter 7, "Nonlinear Spectroscopy for Molecular Structure Determination," R. W. Field *et al.*, Eds., (Blackwell Science, Oxford, 1998), and references therein.; E. W. Schlag, "ZEKE Spectroscopy" (Cambridge University Press, Cambridge, 1998), and references therein.
- 4) K. Suzuki, Y. Emura, S. Ishiuchi and M. Fujii, *J. Electron Spectrosc.* **108**, 13 (2000), K. Suzuki, S. Ishiuchi and M. Fujii, *Faraday Discuss.* **115**, 229 (2000), K. Sakota, N. Yamamoto, K. Ohashi, H. Sekiya, M. Saeki, S. Ishiuchi, M. Sakai and M. Fujii, *Chem. Phys. Lett.* **341**, 70 (2001).
- 5) S. Ishiuchi, M. Saeki, M. Sakai and M. Fujii, *Chem. Phys. Lett.* **322**, 27 (2000).
- 6) M. Saeki, S. Ishiuchi, M. Sakai and M. Fujii, *J. Phys. Chem. A* **105**, 10045 (2001).
- 7) M. Sakai, K. Daigoku, S. Ishiuchi, M. Saeki, K. Hashimoto and M. Fujii, *J. Phys. Chem. A* **105**, 8651 (2001).
- 8) H. Yokoyama, H. Watanabe, T. Omi, S. Ishiuchi and M. Fujii, *J. Phys. Chem. A* **105**, 9366 (2001).
- 9) S. Ishiuchi, M. Sakai, K. Daigoku, T. Ueda, T. Yamanaka, K. Hashimoto and M. Fujii, *Chem. Phys. Lett.* **347**, 87 (2001).

### III-E-1 Photochemistry of Phenol- $(\text{NH}_3)_n$ Clusters: Solvent Effect on a Radical Cleavage of an OH Bond in an Electronically Excited State and Intracuster Reactions in the Product $\text{NH}_4(\text{NH}_3)_{n-1}$ ( $n < 5$ )

DAIGOKU, Kota<sup>1</sup>; ISHIUCHI, Shun-ichi<sup>2</sup>; SAKAI, Makoto<sup>3</sup>; FUJII, Masaaki<sup>4</sup>; HASHIMOTO, Kenro<sup>5</sup>  
(<sup>1</sup>Tokyo Metropolitan Univ.; <sup>2</sup>Tokyo Inst. Tech./JST-PRESTO; <sup>3</sup>Tokyo Inst. Tech.; <sup>4</sup>IMS and Tokyo Inst. Tech.; <sup>5</sup>Tokyo Metropolitan Univ./ACT-JST)

[*J. Chem. Phys.* **119**, 5149–5157 (2003)]

The potential energy surfaces of  $\text{PhOH-(NH}_3)_{0,1}$  and  $\text{NH}_4(\text{NH}_3)_{1-4}$  have been investigated theoretically by *ab initio* methods. Intermolecular stretching in  $\text{PhOH-NH}_3$  assists in the radical cleavage of an OH bond occurring through a  $\pi\pi^*/\pi\sigma^*$  potential crossing. Thus, excited state hydrogen transfer (ESHT) is expected to take place by a solvent-assisted mechanism even in the larger  $\text{PhOH-(NH}_3)_n$ . Because sufficient energy is obtained by ESHT from  $\text{PhOH-(NH}_3)_n$  ( $\pi\pi^*$ ) to  $\text{PhO-NH}_4(\text{NH}_3)_{n-1}$  ( $\pi\sigma^*$ ) ( $n \leq 5$ ), hydrogen relocation and/or ammonia migration in the product  $\text{NH}_4(\text{NH}_3)_{n-1}$  can readily follow ESHT, which is responsible for observing isomer bands in the absorption spectra of the photoinduced reaction products of  $\text{PhOH-(NH}_3)_n$ .

### III-E-2 Four-Color Hole Burning Spectra of Phenol/ammonia 1:3 and 1:4 Clusters

ISHIUCHI, Shun-ichi<sup>1</sup>; DAIGOKU, Kota<sup>2</sup>;

HASHIMOTO, Kenro<sup>3</sup>; FUJII, Masaaki<sup>4</sup>

(<sup>1</sup>Tokyo Inst. Tech./JST-PRESTO; <sup>2</sup>Tokyo Metropolitan Univ.; <sup>3</sup>Tokyo Metropolitan Univ./ACT-JST; <sup>4</sup>IMS and Tokyo Inst. Tech.)

[*J. Chem. Phys.* **120**, 3215–3220 (2004)]

The hole burning spectra of phenol/ammonia (1:3 and 1:4) clusters were measured by a newly developed four-color (UV-near-IR-UV-UV) hole burning spectroscopy, which is a kind of population labeling spectroscopy. From the hole burning spectra, it was found that single species is observed in an  $n = 3$  cluster, while three isomers are observed simultaneously for  $n = 4$ . A possibility was suggested that the reaction efficiency of the hydrogen transfer from the electronically excited phenol/ammonia clusters, which was measured by a comparison with the action spectra of the corresponding cluster, depends on the initial vibronic levels.

### III-E-3 $S_1$ - $S_0$ Electronic Spectrum of Jet-Cooled *m*-Aminophenol

SHINOZAKI, Minako<sup>1</sup>; SAKAI, Makoto<sup>2</sup>;  
YAMAGUCHI, Shigeru<sup>1</sup>; FUJIOKA, Tomoo<sup>1</sup>;  
FUJII, Masaaki<sup>3</sup>

(<sup>1</sup>Tokai Univ.; <sup>2</sup>Tokyo Inst. Tech.; <sup>3</sup>IMS and Tokyo Inst. Tech.)

[*Phys. Chem. Chem. Phys.* **5**, 5044–5050 (2003)]

The  $S_1$  and  $S_0$  states of *m*-aminophenol have been investigated using laser induced fluorescence and

dispersed fluorescence spectroscopy in a supersonic jet. The dispersed fluorescence spectra, obtained by exciting the bands at 34 109 and 34 469  $\text{cm}^{-1}$ , show the same vibronic structure, which suggests the coexistence of rotational isomers in *m*-aminophenol. A quantum chemical calculation also supports the coexistence of rotational isomers. From the relative intensities in the spectrum and the calculated stabilization energies of isomers, the bands are assigned to the origin of the *cis*- and *trans*-isomers, respectively. The dispersed fluorescence spectra obtained by exciting the  $S_1$  vibronic bands were analyzed by comparing with the calculated vibrational frequencies and IR and Raman spectra. From the analysis, the  $S_1$  vibronic bands have been assigned. It was found that a one-to-one correspondence between the  $S_1$  and  $S_0$  vibrations is broken, and vibrational mixing due to Fermi resonance or the Duschinsky effect is suggested.

### III-E-4 Predicted Spatial Resolution of Super-Resolving Fluorescence Microscopy Using Two-Color Fluorescence Dip Spectroscopy

IKETAKI, Yoshinori<sup>1</sup>; WATANABE, Takeshi<sup>2</sup>; ISHIUCHI, Shun-ichi<sup>3</sup>; SAKAI, Makoto<sup>2</sup>; OMATSU, Takashige<sup>4</sup>; YAMAMOTO, Kimihisa<sup>5</sup>; FUJII, Masaaki<sup>6</sup>

(<sup>1</sup>Olympus Optical Co. Ltd.; <sup>2</sup>Tokyo Inst. Tech.; <sup>3</sup>Tokyo Inst. Tech./JST-PRESTO; <sup>4</sup>Chiba Univ.; <sup>5</sup>Keio Univ.; <sup>6</sup>IMS and Tokyo Inst. Tech.)

[*Appl. Spectrosc.* **57**, 1312–1316 (2003)]

The theoretical spatial resolution of the novel super-resolution fluorescence microscopy was investigated. This microscopy is based on the fluorescence depletion process observed by two-color fluorescence dip spectroscopy. For the investigation, we measured the optical properties of Rhodamine 6G concerning the fluorescence depletion process. Using the obtained data, the spatial resolution of the microscopy is theoretically forecast when a first order of the Bessel beam is used for the erase beam. It is found that the resolution overcomes the diffraction limit in the nanometer scale region. The investigation shows that the microscopy gives a spatial resolution better than 100 nm using a nanosecond laser with a pulse energy of  $\sim$  nJ/pulse. The microscopy is expected to be an appropriate novel tool for observing samples with nanometer scale structures.

### III-E-5 Vibrational Energy Relaxation of the 7-Azaindole Dimer in $\text{CCl}_4$ Solution Studied by Picosecond Time-Resolved Transient Fluorescence Detected IR Spectroscopy

SAKAI, Makoto<sup>1</sup>; FUJII, Masaaki<sup>2</sup>

(<sup>1</sup>Tokyo Inst. Tech.; <sup>2</sup>IMS and Tokyo Inst. Tech.)

[*Chem. Phys. Lett.* in press]

The picosecond time-resolved IR spectra of the 7-azaindole dimer in a carbontetrachloride solution was measured by using picosecond time-resolved IR/UV double resonance spectroscopy. This spectroscopy

selectively detects the IR transition by transient fluorescence due to an electronic transition from a vibrationally excited level. The time-evolution of the IR spectrum is a single exponential with a 19 ps lifetime, which does not correspond to fast nonstatistical decay due to the intramolecular vibrational redistribution found in a gas-phase cluster. From a comparison with the time-resolved IR spectrum of a jet-cooled dimer, this decay is assigned to vibrational cooling from the dimer to the solvent.

### III-E-6 Pulsed Field Ionization—ZEKE Photoelectron Spectrum of *o,m,p*-Tolunitrile

SUZUKI, Kazunari<sup>1</sup>; ISHIUCHI, Shun-ichi<sup>2</sup>; SAKAI, Makoto<sup>3</sup>; FUJII, Masaaki<sup>4</sup>

(<sup>1</sup>Waseda Univ.; <sup>2</sup>Tokyo Inst. Tech./JST-PRESTO; <sup>3</sup>Tokyo Inst. Tech.; <sup>4</sup>IMS and Tokyo Inst. Tech.)

[*J. Electron Spectrosc.* in press]

Pulsed field ionization—ZEKE photoelectron spectroscopy has been applied to *o*-, *m*- and *p*-tolunitrile in a supersonic jet. The PFI-ZEKE photoelectron spectra of *m*- and *p*-tolunitrile show well-resolved anharmonic structures in the low frequency region, which are assigned to bands due to internal rotational motion of the methyl group in the cation. Level energies and relative transition intensities are reproduced well by a one-dimensional rotor model with a three-fold axis potential. Potential curves for the internal rotation have been determined. For *o*-tolunitrile, no band due to internal rotation was found in PFI-ZEKE spectrum. It is suggested that the *o*-tolunitrile cation has the high barrier for internal rotation and the stable conformation that is the same as that in  $S_1$  and  $S_0$ . The barrier height and the conformation are compared with other toluene derivatives, and the relation between the electronic character of -CN and the internal rotational motion has been discussed.

### III-E-7 Two-Point-Separation in Super-Resolution Fluorescence Microscope Based on Up-Conversion Fluorescence Depletion Technique

WATANABE, Takeshi<sup>1</sup>; IKETAKI, Yoshinori<sup>2</sup>; OMATSU, Takashige<sup>3</sup>; YAMAMOTO, Kimihisa<sup>4</sup>; SAKAI, Makoto<sup>1</sup>; FUJII, Masaaki<sup>5</sup>

(<sup>1</sup>Tokyo Inst. Tech.; <sup>2</sup>Olympus Optical Co. Ltd.; <sup>3</sup>Chiba Univ.; <sup>4</sup>Keio Univ.; <sup>5</sup>IMS and Tokyo Inst. Tech.)

[*Opt. Express* **11**, 3271–3276 (2003)]

We have demonstrated a realistic super-resolution scanning fluorescence microscope using conventional nanosecond lasers. This super-resolution microscope is based on the combination of two-color fluorescence dip spectroscopy and shape modulation to a doughnut beam. Only by introducing a doughnut erase beam, the resolution of the laser fluorescence microscope breaks the diffraction limit by two times without using any mechanical probe.

### III-E-8 Super-Resolution Fluorescence Microscopy in Nano-Meter Scale Region Using Two-Color Laser Beams

IKETAKI, Yoshinori<sup>1</sup>; WATANABE, Takeshi<sup>2</sup>;  
SAKAI, Makoto<sup>2</sup>; ISHIUCHI, Shun-ichi<sup>3</sup>;  
OMATSU, Takashige<sup>4</sup>; YAMAMOTO, Kimihisa<sup>5</sup>;  
FUJII, Masaaki<sup>6</sup>

(<sup>1</sup>Olympus Optical Co. Ltd.; <sup>2</sup>Tokyo Inst. Tech.; <sup>3</sup>Tokyo Inst. Tech./JST-PRESTO; <sup>4</sup>Chiba Univ.; <sup>5</sup>Keio Univ.; <sup>6</sup>IMS and Tokyo Inst. Tech.)

[*J. Surf. Sci. Soc. Jpn.* **24**, 392–399 (2003)]

A super-resolution fluorescence microscopy using two-color laser beams was proposed. The microscopy is based on the combination of two-color fluorescence dip spectroscopy and a phase modulation technique for the laser beam. By applying the proposed technique to a laser-scanning microscope, a fluorescence image of a sample can be observed with a spatial resolution overcoming the optical diffraction limit. To demonstrate validity of the microscopy, we constructed a scanning microscope system using commercial nano-second pulse lasers. An image of micro beads containing dye molecules was observed by the microscopy. We succeeded in obtaining the image with a resolution overcoming the diffraction limit in nano-meter scale region. The experimental data showed that the resolution was improved three times at least. The microscopy is expected to be an appropriate analysis method for samples with nano-meter scale structure.

### III-E-9 Formation of Doughnut Laser Beam for Super-Resolving Microscopy Using a Phase Spatial Light Modulator

WATANABE, Takeshi<sup>1</sup>; IGASAKI, Yasumori<sup>2</sup>;  
FUKUCHI, Norihiro<sup>2</sup>; SAKAI, Makoto<sup>1</sup>;  
ISHIUCHI, Shun-ichi<sup>3</sup>; FUJII, Masaaki<sup>4</sup>; OMATSU,  
Takashige<sup>5</sup>; YAMAMOTO, Kimihisa<sup>6</sup>; IKETAKI,  
Yoshinori<sup>7</sup>

(<sup>1</sup>Tokyo Inst. Tech.; <sup>2</sup>Hamamatsu Photonics K. K.; <sup>3</sup>Tokyo Inst. Tech./JST-PRESTO; <sup>4</sup>IMS and Tokyo Inst. Tech.; <sup>5</sup>Chiba Univ.; <sup>6</sup>Keio Univ.; <sup>7</sup>Olympus Optical Co. Ltd.)

[*Opt. Eng.* **43**, 1136–1143 (2004)]

The formation of a doughnut-shaped laser beam is presented. To generate the beam, we used an optically addressed parallel-aligned nematic liquid-crystal phase spatial light modulator (PAL-SLM), and observed the shape of the focused beam. By using a compensating technique for wave aberration, the beam had a symmetric doughnut shape with a hole size of  $1\mu\text{m}\phi$  on the focal plane. The experimental result shows that the generated beam can be expected to be applicable to super-resolving microscopy based on the fluorescence depletion process.

## III-F Development of High-Precision Coherent Control and Its Application

Coherent control is based on manipulation of quantum phases of wave functions. It is a basic scheme of controlling a variety of quantum systems from simple atoms to nanostructures with possible applications to novel quantum technologies such as bond-selective chemistry and quantum computation. Coherent control is thus currently one of the principal subjects of various fields of science and technology such as atomic and molecular physics, solid-state physics, quantum electronics, and information science and technology. One promising strategy to carry out coherent control is to use coherent light to modulate a matter wave with its optical phase. We have so far developed a high-precision wave-packet interferometry by stabilizing the relative quantum phase of the two molecular wave packets generated by a pair of fs laser pulses in attosecond time scale. We will apply our high-precision quantum interferometry to gas, liquid, solid, and surface systems to explore and control various quantum phenomena.

### III-F-1 Molecular Wave-Packet Interferometry with Attosecond Quantum Phase Manipulation

OHMORI, Kenji<sup>1</sup>; SATO, Yukinori<sup>2</sup>; NIKITIN, Evgueni E.<sup>3</sup>; RICE, Stuart A.<sup>4</sup>  
(<sup>1</sup>IMS, CREST, JST; <sup>2</sup>Tohoku Univ.; <sup>3</sup>Technion-Israel Inst. Tech.; <sup>4</sup>Univ. Chicago)

[*Phys. Rev. Lett.* **91**, 243003 (4 pages) (2003)]

Wave packet (WP) interferometry is a clear manifestation of wave nature of matter, and is a basic scheme of controlling a variety of quantum systems from simple atoms to nano structures with possible applications to novel quantum technologies such as bond-selective chemistry and quantum computation. The key technique in the WP interferometry is fine tuning of the delay between two light pulses that produce a pair of WP's with a precision far better than the quantum oscillation cycle of the WP's, say few femtoseconds (fs) to attoseconds (as). The WP's are then phase-locked and produce stable interference. We have constructed an "attosecond phase modulator (APM)": a device for tuning the delay  $\tau$  between two UV fs pulses with attosecond stability and resolution. We have utilized this APM to create an unprecedented high-precision WP interferometer with a dilute ensemble of the HgAr van der Waals complex; our interferometer displayed almost 100% fringe contrast as a function of the delay  $\tau$  between two UV fs pulses at 254 nm ( $\rightarrow$  Figure 1). Moreover we have demonstrated the dephasing and rephasing of the interferograms of consecutive vibrational eigenstates within WP's, which arise from a subtle difference in the quantum oscillation cycles of each eigenstates, different from the well-known collapse and revival of the electron WP's in atoms.<sup>1)</sup> Our high precision interferometer makes it possible to create virtually arbitrary relative superpositions of the three vibrational eigenstates within a WP only by tuning a single parameter  $\tau$ . It is pointed out that the interference structure can be retrieved from the population information stored in the thermal ensemble of molecules even after the coherence is wiped out ( $\rightarrow$  Figure 2). All these features are quite general in WP interference and therefore provide basis for opening new perspective of coherent control in a wide variety of quantum systems.

#### Reference

1) John A. Yeazell, Mark Mallalieu and C. R. Stroud, Jr., *Phys. Rev. Lett.* **64**, 2007 (1990).

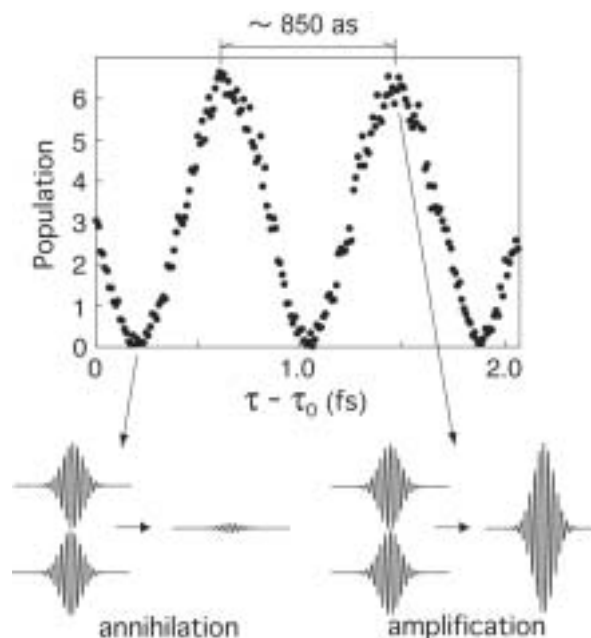


**Figure 1.** An example of the quantum interferograms of two molecular wave packets moving on the  $A(^3\text{O}^+)$ -state potential curve of the Hg-Ar vdW complex. The interferogram displays almost 100% fringe contrast as a function of the inter-pulse delay  $\tau$  tuned with attosecond stability and resolution. Its top and bottom represent amplification and annihilation of the wave packet.

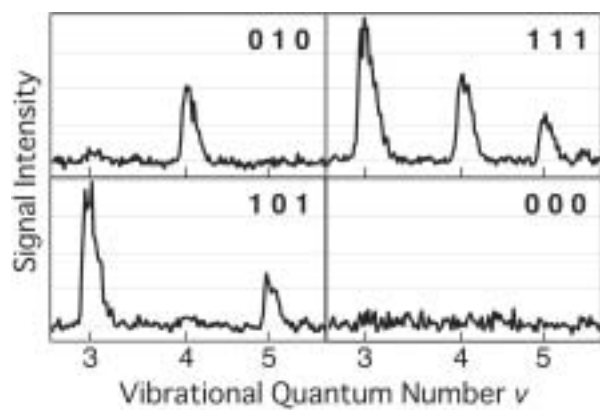


**Figure 2.** Population codes written in a Hg-Ar vdW complex by using wave-packet interference. Particular information can be encoded as a relative superposition of the vibrational eigenstates within a wave packet, and that information can be retrieved as a population code stored in the ensemble of molecules even after the coherence is wiped out.

## III-G Structure and Properties of Carbon Nanotubes and Nanohorns

Our research on single-wall carbon nanotubes (SWNTs) and single-wall carbon nanohorns (SWNHs) have been extending toward two directions, the analysis of nanometer-scaled structures and the application. Developing new types of transmission electron microscopes (TEM), we could, for the first time, clearly observed holes opened on the tube walls. Also Gd atoms attached at the open end of the tubes and single-carbon-atom defects on the tube walls became observable. Even the determination of chiralities of SWNTs was possible. With aids of these TEM techniques, several methods of encapsulation and de-encapsulation of various molecules and clusters in liquid phase at room temperature have been developed, which assure the future application of SWNTs and SWNHs particularly in biological use.

Application of SWNTs was greatly enhanced by the progress of growth method, that is, site-selective growth by chemical vapor deposition. A top-gate transistor was fabricated and its performances has been ranked at the world top record for some time. For practical realization of SWNT-devices, we need to develop highly refined growth-methods, which we are currently engaging in.

### III-G-1 Direct Evidence for Atomic Defects in Graphene Layers

**HASHIMOTO, Ayako<sup>1</sup>; SUENAGA, Kazutomo<sup>1</sup>; GLOTER, Alexandre<sup>1</sup>; URITA, Koki<sup>1,2</sup>; IJIMA, Sumio<sup>1,3,4,5,6</sup>**  
(<sup>1</sup>AIST; <sup>2</sup>Chiba Univ.; <sup>3</sup>JST; <sup>4</sup>NEC; <sup>5</sup>Meijo Univ. <sup>6</sup>IMS)

[*Nature* **430**, 870–873 (2004)]

Atomic-scale defects in graphene layers alter the physical and chemical properties of carbon nanostructures. Theoretical predictions have recently shown that energetic particles such as electrons and ions can induce polymorphic atomic defects in graphene layers as a result of knock-on atom displacements. However, the number of experimental reports on these defects is limited. The graphite network in single-walled carbon nanotubes has been visualized by transmission electron microscopy (TEM) and their chiral indices have been determined. But the methods used require a long image acquisition time and intensive numerical treatments after observations to find an ‘average’ image, which prevents the accurate detection and investigation of defect structures. Here we report observations in situ of defect formation in single graphene layers by high-resolution TEM. The observed structures are expected to be of use when engineering the properties of carbon nanostructures for specific device applications.

### III-G-2 Selective Deposition of a Gadolinium (III) Cluster in a Hole Opening of Single-Wall Carbon Nanohorn

**HASHIMOTO, Ayako<sup>1</sup>; YORIMITSU, Hideki<sup>2</sup>; AJIMA, Kumiko<sup>3</sup>; SUENAGA, Kazutomo<sup>1</sup>; ISOBE, Hiroyuki<sup>2</sup>; MIYAWAKI, Jin<sup>3</sup>; YUDASAKA, Masako<sup>3</sup>; IJIMA, Sumio<sup>1,3,4,5,6</sup>; NAKAMURA, Eiichi<sup>2</sup>**  
(<sup>1</sup>AIST; <sup>2</sup>Univ. Tokyo; <sup>3</sup>JST; <sup>4</sup>NEC; <sup>5</sup>Meijo Univ.; <sup>6</sup>IMS)

[*Proc. Natl. Acad. Sci.* **101**, 8527–8530 (2004)]

As has been amply demonstrated in chemistry by way of metal-catalysis, metal-complexation should

immensely widen the scope of carbon cluster science. Thus, metal-containing hollow carbon clusters such as endohedral metallofullerenes and carbon nanotube filled with metal atoms have been suggested as promising materials. However, the methodology to rationally control the size and the location of the metal clusters as well as to ensure high yield production of the material on a large scale has been lacking. Herein we report a method for forming a one- to multi-atom metal cluster specifically at the hydrophilic hole opening of a carbon nanotube as demonstrated by deposition of Gd(OAc)<sub>3</sub> in single-wall carbon nanohorns. The hole-selective deposition of the Gd atoms allows atomic scale detection of the structural defect in the graphitic materials, and, on a bulk scale, controls the permeability of molecules through the holes. The result would find use for modulation of the electronic properties of carbon nanotubes.

### III-G-3 Material Storage Mechanism in Porous Nanocarbon

**AJIMA, Kumiko<sup>1</sup>; YUDASAKA, Masako<sup>2</sup>; SUENAGA, Kazutomo<sup>3</sup>; KASUYA, Daisuke<sup>2</sup>; AZAMI, Takeshi<sup>2</sup>; IJIMA, Sumio<sup>1,2,3,4,5</sup>**  
(<sup>1</sup>JST; <sup>2</sup>NEC; <sup>3</sup>AIST; <sup>4</sup>Meijo Univ.; <sup>5</sup>IMS)

[*Adv. Mater.* **16**, 397–401 (2004)]

Carbonaceous materials, such as activated carbon and charcoal, have long been known to possess “nanospaces,” where a variety of materials can be accommodated. Their structures and chemical properties, however, have never been optimized for any specific purpose, because their mechanism of storing objects is not yet fully understood. We have therefore attempted to visualize how materials is stored in the inner spaces of nanocarbon materials in order to verify the storage mechanism. We used “single-walled carbon nanohorns” (SWNHs) for this purpose. This porous nanocarbon material, composed of single layer/crystal/atom graphite walls, is known to possess completely enclosed nanoscale spaces, and is therefore quite suitable for these experiments.

### III-G-4 Structural Evolutions of Carbon Nano-Peapods under Electron Microscopic Observation

GLOTER, Alexandre<sup>1</sup>; SUENAGA, Kazutomo<sup>1</sup>; KATAURA, Hiromichi<sup>2</sup>; FUJII, Ryosuke<sup>2</sup>; KODAMA, Takeshi<sup>2</sup>; NISHIKAWA, Hiroyuki<sup>2</sup>; IKEMOTO, Isao<sup>2</sup>; KIKUCHI, Koichi<sup>2</sup>; SUZUKI, Shinzo<sup>2</sup>; ACHIBA, Yohji<sup>2</sup>; IJIMA, Sumio<sup>1,3,4,5,6</sup> (<sup>1</sup>AIST; <sup>2</sup>Tokyo Metropolitan Univ.; <sup>3</sup>Meijo Univ.; <sup>4</sup>JST; <sup>5</sup>NEC; <sup>6</sup>IMS)

[*Chem. Phys. Lett.* **390**, 462–466 (2004)]

Supramolecular assemblages made of single wall carbon nanotubes (SWNT) filled with fullerenes or metal doped fullerenes exhibit promising electronic structure variations at a nanometer scale. Nevertheless, the knowledge about the structural defects of these systems is still very limited. Here, we report structural evolutions under high-resolution electron microscopic observation at the sensitivity of a single atom detection for Ca@C<sub>82</sub> molecules encapsulated within SWNT.

### III-G-5 Nano-Extraction and Nano-Condensation for C<sub>60</sub> Incorporation into Single-Wall Carbon Nanotubes in Liquid Phases

YUDASAKA, Masako<sup>1</sup>; AJIMA, Kumiko<sup>2</sup>; SUENAGA, Kazutomo<sup>3</sup>; ICHIHASHI, Toshinari<sup>1</sup>; HASHIMOTO, Ayako<sup>3</sup>; IJIMA, Sumio<sup>1,2,3,4,5</sup> (<sup>1</sup>NEC; <sup>2</sup>JST; <sup>3</sup>AIST; <sup>4</sup>Meijo Univ.; <sup>5</sup>IMS)

[*Chem. Phys. Lett.* **380**, 42–46 (2003)]

We have established two new methods that enable incorporation of guest molecules into single-wall carbon nanotubes in liquid phases; nano-extraction and nano-condensation methods. To make SWNTs that have incorporated C<sub>60</sub> ((C<sub>60</sub>)<sub>n</sub>@SWNT) through nano-extraction, we put C<sub>60</sub> and SWNTs in ethanol for 1 day during which the C<sub>60</sub> molecules deposited themselves inside the SWNTs. The incorporation mechanism appears to be that the C<sub>60</sub> molecules dissolved slightly in the ethanol, diffused toward the SWNTs, and eventually deposited themselves at the most stable sites—that is, inside the SWNTs. In the case of nano-condensation, we formed thin layers of C<sub>60</sub>-toluene saturated solution on SWNT surfaces, and then obtained (C<sub>60</sub>)<sub>n</sub>@SWNT within a few seconds. A reasonable explanation is that the C<sub>60</sub> molecules migrated through the thin layers of the toluene-C<sub>60</sub> mixtures on the SWNT surfaces and finally deposited themselves inside the SWNTs.

### III-G-6 Preferential Deposition of Pt Nanoparticles inside Single-Wall Carbon Nanohorns

YUGE, Ryota<sup>1</sup>; ICHIHASHI, Toshinari<sup>1</sup>; SHIMAKAWA, Yuichi<sup>1</sup>; KUBO, Yoshimi<sup>1</sup>; YUDASAKA, Masako<sup>1</sup>; IJIMA, Sumio<sup>1,2,3,4,5</sup> (<sup>1</sup>NEC; <sup>2</sup>JST; <sup>3</sup>AIST; <sup>4</sup>Meijo Univ.; <sup>5</sup>IMS)

[*Adv. Mater.* **16**, 1420–1423 (2004)]

Many types of materials can be incorporated into one-dimensional (1D) spaces of carbon nanotubes (CNTs). CNTs having fullerenes in their insides, “peapods,” are well known, and ionic salts, Ga, and organic molecules are also successfully incorporated. This 1D ordering is unique and fascinating but it is too simple to cope with a variety of application demands. Therefore we propose to use three-dimensional nano-spaces of single-wall carbon nanohorns (SWNHs). Here, we report that our strategy is promising, that is, Pt nanoparticles could be placed inside this space. Furthermore, a curious size-mismatch is noticed, that is, the Pt particle diameters are large, but no holes with such diameters can be seen, which remind us ships-in-bottles. The formation mechanism of the Pt particle reveals that the starting materials are first incorporated into the SWNHs perhaps through the small wall-holes, and they construct the Pt-particles inside the SWNHs.

### III-G-7 Support Materials Based on Converted Aluminum Films for Chemical Vapor Deposition Growth of Single-Wall Carbon Nanotubes

HONGO, Hiroo<sup>1</sup>; NIHEY, Fumiyuki<sup>1</sup>; ICHIHASHI, Toshinari<sup>1</sup>; OCHIAI, Yukinori<sup>1</sup>; YUDASAKA, Masako<sup>1</sup>; IJIMA, Sumio<sup>1,2,3,4</sup> (<sup>1</sup>NEC; <sup>2</sup>JST; <sup>3</sup>Meijo Univ.; <sup>4</sup>IMS)

[*Chem. Phys. Lett.* **380**, 158–164 (2003)]

We systematically studied the support materials for chemical vapor deposition of single-wall carbon nanotubes (SWNTs). Four support materials with iron catalysts were investigated: silicon dioxide, aluminum film, boehmite, and g-alumina. The boehmite and the  $\gamma$ -alumina were progressively converted from evaporated aluminum film. The iron catalysts on the aluminum film, the boehmite, and the  $\gamma$ -alumina produced a good SWNT yield in the growth temperature range of 650–800 °C, while the catalysts on silicon dioxide produced a poor SWNT yield. The X-ray diffraction patterns suggested that the catalyst particle sizes were kept small on these aluminum-based support materials.

### III-G-8 Fe-Sapphire and C-Fe-Sapphire Interactions and Their Effect on the Growth of Single-Walled Carbon Nanotubes by Chemical Vapor Deposition

YUDASAKA, Masako<sup>1</sup>; KASUYA, Yohko<sup>2</sup>; JING, Fan<sup>1</sup>; ZHANG, Minfang<sup>1</sup>; IJIMA, Sumio<sup>1,2,3,4,5</sup> (<sup>1</sup>NEC; <sup>2</sup>JST; <sup>3</sup>Meijo Univ.; <sup>4</sup>AIST; <sup>5</sup>IMS)

[*J. Nanosci. Nanotechnol.* **4**, 1–5 (2004)]

We previously reported that the quantity of single-walled carbon nanotubes grown on Fe-coated sapphire by chemical vapor deposition depended on the crystallographic faces of sapphires. In this report, we show that the interaction of Fe, sapphire, and carbon depended on the sapphire faces. We deduce that the quantity of Fe available to catalyze the growth of single-walled carbon nano-tubes was suppressed by the formation of Fe-Al alloys and whether the Fe-Al alloys were formed on Fe-

coated sapphire or not depended on the sapphire-surface structure.

### III-G-9 Carbon-Nanotubes Field-Effect Transistors with Very High Intrinsic Transconductance

NIHEY, Fumiuyuki<sup>1</sup>; HONGO, Hiroo<sup>1</sup>; OCHIAI, Yukinori<sup>1</sup>; YUDASAKA, Masako<sup>1</sup>; IJIMA, Sumio<sup>1,2,3,4</sup>

(<sup>1</sup>NEC; <sup>2</sup>JST; <sup>3</sup>Meijo Univ.; <sup>4</sup>IMS)

[*Jpn. J. Appl. Phys.* **42**, L1288–L1291 (2003)]

We investigated intrinsic transconductance of carbon-nanotube field-effect transistors (CNT-FETs) with carbon nanotubes (CNTs) grown by chemical vapor deposition. The measured transconductance at a drain voltage of  $-1$  V was  $8.7 \mu\text{S}$  for a CNT with a diameter of  $1.5$  nm. Very high intrinsic transconductance of  $20 \mu\text{S}$  was estimated by considering the contribution of parasitic resistance. Apparent and intrinsic transconductance per unit channel width were  $5800 \mu\text{S}/\mu\text{m}$  and  $13000 \mu\text{S}/\mu\text{m}$ , respectively, which are enormously larger than those for the state-of-the-art Si-MOSFETs. The parasitic resistance is dominated by the resistance of CNT in the region between the gate and contact. We expect the performance of CNTFETs will further advance by improving CNT quality and by optimizing device structures.

### III-G-10 Raman Scattering Study on Fullerene Derived Intermediates Formed within Single-Wall Carbon Nanotube: From Peapod to Double-Wall Carbon Nanotube

BANDOW, Shunji<sup>1</sup>; HIRAOKA, Tatsuki<sup>1</sup>; YUMURA, Takashi<sup>1</sup>; HIRAHARA, Kaori<sup>1</sup>; SHINOHARA, Hisanori<sup>2</sup>; IJIMA, Sumio<sup>1,3,4,5</sup>

(<sup>1</sup>Meijo Univ.; <sup>2</sup>Nagoya Univ.; <sup>3</sup>NEC; <sup>4</sup>JST; <sup>5</sup>IMS)

[*Chem. Phys. Lett.* **384**, 320–325 (2004)]

By heating of  $\text{C}_{60}$  peapods at  $900$  °C in vacuum, eight or more Raman peaks associated with the inner tubes were observed in the frequency range of the radial breathing mode vibration. An analysis of time traces of the peak intensities led to the growing mechanism of double-wall nanotubes: inner tubes with  $\approx 0.7$  nm diameters are first formed and then increase their diameters. To explain these phenomena, we propose a model based on formation of short achiral zig-zag nanotubes in the beginning of  $\text{C}_{60}$  coalescence.

### III-G-11 Evidence for Substantial Interaction between Gd Ion and SWNT in (Gd@C<sub>82</sub>)@SWNT Peapods Revealed by STM Studies

KIMURA, K.<sup>1</sup>; IKEDA, N.<sup>1</sup>; MARUYAMA, Yusei<sup>1</sup>; OKAZAKI, Toshiya<sup>2</sup>; SHINOHARA, Hisanori<sup>2</sup>; BANDOW, Shunji<sup>3</sup>; IJIMA, Sumio<sup>3,4,5,6</sup>

(<sup>1</sup>Hosei Univ.; <sup>2</sup>Nagoya Univ.; <sup>3</sup>Meijo Univ.; <sup>4</sup>NEC; <sup>5</sup>JST; <sup>6</sup>IMS)

[*Chem. Phys. Lett.* **379**, 340–344 (2003)]

A metallofullerene,  $\text{Gd@C}_{82}$ , encapsulated in the inside of single walled carbon nanotube (SWNT) has been identified as an STM image of a carbon cage and a Gd atom by a measurement of the tunnel currents onto the SWNT surface. This fact indicates that there is a substantial local interaction between the wall of SWNT and the Gd ions close to the wall. The origin of this interaction is not yet clear, but its existence has also been supported by the results of axially- and peripherally-resolved STS measurements around the Gd ion sites in the peapod.

### III-G-12 Structure Changes of Single-Wall Carbon Nanotubes and Single-Wall Carbon Nanohorns Cued by Heat Treatment

YUDASAKA, Masako<sup>1</sup>; ICHIHASHI, Toshinari<sup>1</sup>; KASUYA, Daisuke<sup>1</sup>; KATAURA, Hiromichi<sup>2</sup>; IJIMA, Sumio<sup>1,3,4,5</sup>

(<sup>1</sup>NEC; <sup>2</sup>Tokyo Metropolitan Univ.; <sup>3</sup>JST; <sup>4</sup>Meijo Univ.; <sup>5</sup>IMS)

[*Carbon* **41**, 1273–1280 (2003)]

Raman spectra and transmission electron microscope images showed that diameter enlargement of HiPco, a kind of single-wall carbon nanotubes, accompanied by tube-wall corrugation was caused by heat treatment (HT) at  $1000$  to  $1700$  °C. Further enlargement accompanied by straightening of the tube walls and incorporation of carbon fragments within the tubes became obvious after HT at  $1800$  to  $1900$  °C. The transformation of some single-wall carbon nanotubes into multi-wall nanotubes was observed after HT at  $2000$  °C, and most single-wall tubes were transformed into multi-wall ones by HT at  $2400$  °C. What influence the Fe contained in the HiPco tubes had on these structure changes was unclear; similar changes were observed in single-wall carbon nanohorns that did not contain any metal. This indicates that thermally induced changes in the structure of single-wall carbon nanotubes can occur without a metal catalyst. Heat treatment increased the integrity of the nanotube-papers, and this increase may have been due to tube-tube interconnections created by HT.

### III-G-13 Diameter Enlargement of Single-Wall Carbon Nanotubes by Oxidation

ZHANG, Minfang<sup>1</sup>; YUDASAKA, Masako<sup>2</sup>; IJIMA, Sumio<sup>1,2,3,4,5</sup>

(<sup>1</sup>JST; <sup>2</sup>NEC; <sup>3</sup>AIST; <sup>4</sup>Meijo Univ.; <sup>5</sup>IMS)

[*J. Phys. Chem. B* **108**, 149–153 (2004)]

The diameter of high-pressure CO (HiPco) single-wall carbon nanotubes (SWNTs) has been enlarged by treating them with nitric acid and oxygen, and the diameter enlargement is related to the nitric acid refluxing time. Raman spectra (exciting wavelength  $488$  nm) and transmission electron microscopy showed that the  $0.8$ – $1.2$  nm diameter distribution of HiPco SWNTs could be narrowed to one centered around  $1.2$  nm when

the nitric acid treatment time was 1 h. Significantly, SWNTs of 1.37–2.4 nm in diameter were discovered when the nitric acid treatment lasted more than 2 h.

### III-G-14 A Theoretical Study on the Geometrical Features on Finite-Length Carbon Nanotubes Capped with Fullerenes Hemisphere

YUMURA, Takashi<sup>1</sup>; HIRAHARA, Kaori<sup>1</sup>; BANDOW, Shunji<sup>1</sup>; YOSHIZAWA, Kazunari<sup>2</sup>; IJIMA, Sumio<sup>1,3,4,5,6</sup>  
(<sup>1</sup>Meijo Univ.; <sup>2</sup>Kyushu Univ.; <sup>3</sup>NEC; <sup>4</sup>JST; <sup>5</sup>AIST; <sup>6</sup>IMS)

[*Chem. Phys. Lett.* **386**, 38–43 (2004)]

The structures of the finite-length (5,5) and (9,0) carbon nanotubes capped with fullerene hemisphere are analyzed by quantum chemical calculations at the B3LYP DFT level of theory. DFT calculations demonstrate that the geometries of the armchair tubes depend on the number of cyclic *cis*-polyene chains lined up along the tube axis, whereas the zigzag tubes consist of Kekulé-type networks in the cylinder, the geometries being independent of the number of component cyclic *trans*-polyene chains.

### III-G-15 The Role of Fullerene Hemisphere in Determining the Geometrical Features of Finite-Length Carbon Nanotubes

YUMURA, Takashi<sup>1</sup>; BANDOW, Shunji<sup>1</sup>; YOSHIZAWA, Kazunari<sup>2</sup>; IJIMA, Sumio<sup>1,3,4,5,6</sup>  
(<sup>1</sup>Meijo Univ.; <sup>2</sup>Kyushu Univ.; <sup>3</sup>NEC; <sup>4</sup>JST; <sup>5</sup>AIST; <sup>6</sup>IMS)

[*J. Phys. Chem. B* **108**, 11426–11434 (2004)]

Geometrical and electronic features of the armchair C<sub>40+20n</sub> and zigzag C<sub>42+18n</sub> nanotubes, in which *n* is the number of cyclic *cis*- and *trans*-polyene chains involved in the nanotubes, are analyzed from density functional theory (DFT) calculations. To illuminate the role of the fullerene hemispheres in their structures, C<sub>20n</sub>H<sub>20</sub>, and C<sub>18n</sub>H<sub>18</sub>, are also studied in terms of orbital interactions. Although there are various bond-deformation patterns within the *cis*-polyene chains in the C<sub>20n</sub>H<sub>20</sub> series, the C<sub>40+20n</sub> series always have similar bond-length alternate patterns. The geometrical change in the capped nanotubes is a consequence of orbital interactions in the cylindrical segments with the fullerene hemispheres. Accordingly, the fullerene hemispheres play a dominant role in determining the geometrical and electronic properties of the capped nanotubes. DFT calculations also demonstrate that the geometries of the armchair series exhibit an oscillatory behavior as the chain width with a periodicity of 3.

### III-G-16 A Catalytic Chemical Vapor Deposition Synthesis of Double-Walled Carbon Nanotubes over Metal Catalysts Supported on a Mesoporous Material

ZHU, Jin<sup>1</sup>; YUDASAKA, Masako<sup>2</sup>; IJIMA,

Sumio<sup>1,2,3,4,5</sup>  
(<sup>1</sup>JST; <sup>2</sup>NEC; <sup>3</sup>AIST; <sup>4</sup>Meijo Univ.; <sup>5</sup>IMS)

[*Chem. Phys. Lett.* **380**, 496–502 (2003)]

Double-walled carbon nanotubes (DWNTs) have been synthesized by catalytic chemical vapor deposition (CCVD) over supported metal catalysts decomposed from Fe(CH<sub>3</sub>COO)<sub>2</sub> and Co(CH<sub>3</sub>COO)<sub>2</sub> on mesoporous silica. Bundles of tubes with relatively high percentage of DWNTs, in areas where tubular layered structures could be clearly resolved, have been observed by transmission electron microscopy (TEM). In other areas, crystal-like alignment of very uniform DWNTs was observed for the first time, suggesting that mesoporous silica might play a templating role in guiding the initial nanotube growth. In addition, compatible with nanoelectronics research, bridging of catalytic islands by DWNTs has also been demonstrated.

### III-G-17 Controlled Opening of Single-Wall Carbon Nanohorns by Heat Treatment in Carbon Dioxide

BEKYAROVA, Elena<sup>1</sup>; KANEKO, Katsumi<sup>1</sup>; YUDASAKA, Masako<sup>2</sup>; KASUYA, Daisuke<sup>2</sup>; IJIMA, Sumio<sup>2,3,4,5</sup>; HUDOBRO, Ana<sup>6</sup>; RODRIGUEZ-REINOSO, Francisco<sup>6</sup>  
(<sup>1</sup>Chiba Univ.; <sup>2</sup>NEC; <sup>3</sup>JST; <sup>4</sup>Meijo Univ.; <sup>5</sup>IMS; <sup>6</sup>Univ. Alicante)

[*J. Phys. Chem. B* **107**, 4479–4484 (2003)]

The opening of *bud*-type single-wall carbon nanohorns (SWNHs) by heat treatment in CO<sub>2</sub> was studied by TEM and nitrogen adsorption (77 K). The adsorption isotherms indicate that oxidation by CO<sub>2</sub> at 1273 K provides a sufficient nanohorn opening. The pore parameters of the open nanohorns can be controlled by varying the treatment conditions; the size of the generated nanopores increases with the temperature and time of treatment. In addition, TPD experiments indicate a significant decrease of the oxygen content in SWNHs opened by heat treatment in CO<sub>2</sub>. This is in contrast to the procedures reported in the literature for opening of carbon nanotubular structures, typically introducing oxygen functional groups.

### III-G-18 Interstitial Nanopore Change of Single Wall Carbon Nanohorn Assemblies with High Temperature Treatment

OHBA, Tomonori<sup>1</sup>; OMORI, Takumi<sup>1</sup>; KANO, Hirofumi<sup>1</sup>; YUDASAKA, Masako<sup>2</sup>; IJIMA, Sumio<sup>2,3,4,5</sup>; KANEKO, Katsumi<sup>1</sup>  
(<sup>1</sup>Chiba Univ.; <sup>2</sup>NEC; <sup>3</sup>Meijo Univ.; <sup>4</sup>JST; <sup>5</sup>IMS)

[*Chem. Phys. Lett.* **389**, 332–336 (2004)]

Single-wall carbon nanohorns (SWNHs) were treated in vacuum at different temperatures of 473 to 1073 K. The nanostructural change due to the heat-treatment was studied by adsorption of N<sub>2</sub> at 77 K and H<sub>2</sub>O at 303 K. The determined particle density showed that gas is

not adsorbed in internal pores, but in interstitial pores. The high temperature treatment (HTT) in vacuo changed water adsorption, but it gave almost no influence on N<sub>2</sub> adsorption. The maximum nanopore volume from H<sub>2</sub>O adsorption was observed at 673 K, indicating the interstitial nanopore change due to a local orientational change of SWNH particles.

### III-G-19 Direct Thermal Fluorination of Single Wall Carbon Nanohorns

HATTORI, Yoshiyuki<sup>1</sup>; KANO, Hirofumi<sup>1</sup>; OKINO, Fujio<sup>2</sup>; TOUHARA, Hidekazu<sup>2</sup>; KASUYA, Daisuke<sup>3</sup>; YUDASAKA, Masako<sup>3</sup>; IJIMA, Sumio<sup>3,4,5</sup>; KANEKO, Katsumi<sup>1</sup>

(<sup>1</sup>Chiba Univ.; <sup>2</sup>Shinshu Univ.; <sup>3</sup>NEC; <sup>4</sup>JST; <sup>5</sup>Meijo Univ.; <sup>6</sup>AIST; <sup>7</sup>IMS)

[*J. Phys. Chem. B* **108**, 9614–9618 (2004)]

Single wall carbon nanohorns (SWNHs) were fluorinated to form more attractive nanohorns that have the characteristic structural and adsorptive properties. Nitrogen adsorption, XPS, TEM studies elucidated the surface states and the morphologies of fluorinated SWNHs (F-SWNHs). The XPS results of F-SWNHs showed that the nature of C–F bonds changed from semi-ionic to covalent with increase of the fluorination temperature. The N<sub>2</sub> adsorption isotherm indicated that the total amounts of N<sub>2</sub> adsorption on SWNHs fluorinated at 303 and 373 K was smaller than that of pristine SWNHs. After fluorination at 473 K, nano-order windows were produced on the sidewalls of SWNHs without change in the shape of each horn and aggregate. Therefore, the SWNHs fluorinated at 473 K can adsorb N<sub>2</sub> molecules on the internal surfaces of nanohorns through the nanowindows.

### III-G-20 Synthesis of Carbon Nanohorn Particles by Simple Pulsed Arc Discharge Ignited between Pre-Heated Carbon Rods

YAMAGUCHI, Takashi<sup>1</sup>; BANDOW, Shunji<sup>1</sup>; IJIMA, Sumio<sup>1,2,3,4,5</sup>

(<sup>1</sup>Meijo Univ.; <sup>2</sup>NEC; <sup>3</sup>AIST; <sup>4</sup>JST; <sup>5</sup>IMS)

[*Chem. Phys. Lett.* **389**, 181–185 (2004)]

Single-wall carbon nanohorn (SWNH) particles were generated by simple pulsed arc discharge between pure carbon rods in the atmospheric pressure of air. Purity of SWNHs was reached higher than 90%, and the heating in dry air at 500 °C was useful for removal of amorphous carbon. The mean size of SWNH particles was ≈ 50 nm, which is smaller than those prepared by the CO<sub>2</sub> laser method. Pre-heating of the carbon rod up to 1000 °C, conducted just before ignition of arc, improved the quality of SWNHs. Transmission electron microscopy, scanning electron microscopy and Raman spectroscopy were used to characterize these SWNH particles.

### III-G-21 Solvent Effects on Hole-Edge Structure for Single-Wall Carbon Nanotubes and Single-Wall Carbon Nanohorns

MIYAWAKI, Jin<sup>1</sup>; YUDASAKA, Masako<sup>2</sup>; IJIMA, Sumio<sup>1,2,3,4,5</sup>

(<sup>1</sup>JST; <sup>2</sup>NEC; <sup>3</sup>AIST; <sup>4</sup>Meijo Univ.; <sup>5</sup>IMS)

[*J. Phys. Chem. B* **108**, 10732–10735 (2004)]

To extend the application fields of single-wall carbon nanotubes (SWNTs) and single-wall carbon nanohorns (SWNHs), their chemical modification is essential. Since their graphene-sheet-based structures are chemically robust, only the edges of the graphene sheets, more specifically the oxygen-containing functional groups at hole edges, are useful sites for chemical modification. However, not much is known about the hole-edges, so the phenomenon reported here, that the hole edges easily react with conventional reagents, was previously unknown. We observed a lowering of the combustion temperature of SWNTs and SWNHs immersed in water; this lowering was induced as a result of the hydrolysis of oxygen-containing functional groups (anhydrides and/or lactones) at the hole edges. We also found that the reactivity of hole edges can be easily controlled through an appropriate choice of solvents. We believe that this study is helpful to our understanding of hole-edge chemistry and will help to enable the production of well-designed carbonaceous materials with high functionality.

### III-G-22 Evidence for the Intermolecular Motion of Gd Atoms in a Gd<sub>2</sub>@C<sub>92</sub> Nanopeapod

SUENAGA, Kazutomo<sup>1</sup>; TANIGUCHI, Risa<sup>2</sup>; SHIMADA, Takashi<sup>2</sup>; OKAZAKI, Toshiya<sup>2</sup>; SHINOHARA, Hisanori<sup>2</sup>; IJIMA, Sumio<sup>1,3,4,5</sup>

(<sup>1</sup>AIST; <sup>2</sup>Nagoya Univ.; <sup>3</sup>NEC; <sup>4</sup>Meijo Univ.; <sup>5</sup>IMS)

[*Nano Lett.* **3**, 1395–1398 (2003)]

Atoms in a confined space can be regarded to represent a completely new phase because it should behave differently than the atoms in a solid or in a free-space. The metallofullerene provides an ideal case of the confined atoms since a number of metal atoms are imprisoned in a subnanometer void of the carbon cage. Here we give direct evidence of the dynamic behavior for the confined atoms in metallofullerenes by observing individual atoms using the high-resolution transmission electron microscopy. Rapid movement of Gd atoms in Gd<sub>2</sub>@C<sub>92</sub> peapod is identified for the first time. By comparison with simulation, the amplitude of the motion is roughly quantified as 0.2 nm at room temperature and is reduced to almost half at 100 K.

### III-G-23 Laser Vaporization Synthesis of Polyhedral Graphite

KOKAI, Fumio<sup>1</sup>; TAKAHASHI, Kunimitsu<sup>2</sup>; KASUYA, Daisuke<sup>3</sup>; NAKAYAMA, Atsuko<sup>4</sup>; KOGA, Yoshinori<sup>4</sup>; YUDASAKA, Masako<sup>3</sup>; IJIMA, Sumio<sup>3,4,5,6</sup>

(<sup>1</sup>Mie Univ.; <sup>2</sup>IRI; <sup>3</sup>NEC; <sup>4</sup>AIST; <sup>5</sup>Meijo Univ.; <sup>6</sup>IMS)

[*Appl. Phys. A: Mater. Sci. Process.* **77**, 69–71 (2003)]

Polyhedral graphite (PG) particles have been synthesized by CO<sub>2</sub> laser vaporization of graphite in high-pressure Ar gas ( $8 \times 10^5$  Pa). Faceted PG particles, ranging in size from 110 to 150 nm, have a turbostratic structure. The yield of PG is more than 90%. This synthesis is based on the condensation of hot carbon species confined by an Ar-gas atmosphere.

### III-G-24 Direct Observation of 3D Mesoporous Structure by Scanning Electron Microscopy (SEM): SBA-15 Silica and CMK-5 Carbon

CHE, Shunai<sup>1</sup>; LUND, Kristina<sup>2</sup>; TATSUMI, Takashi<sup>1</sup>; IJIMA, Sumio<sup>3,4,5,6</sup>; JOO, Sang Hoon<sup>7</sup>; RYOO, Ryong<sup>7</sup>; TERASAKI, Osamu<sup>8</sup>

(<sup>1</sup>Yokohama Natl. Univ.; <sup>2</sup>Stockholm Univ.; <sup>3</sup>JST; <sup>4</sup>NEC; <sup>5</sup>Meijo Univ.; <sup>6</sup>IMS; <sup>7</sup>Korea Adv. Inst. Sci. Tech.; <sup>8</sup>Tohoku Univ.)

[*Angew. Chem., Int. Ed.* **42**, 2182–2185 (2003)]

Mesoporous silica has attracted much attention in recent years, due to new possibilities for advanced applications in catalysis, separation technologies, electronic engineering, and manufacturing of optic devices. The highly nanoporous structures with good thermochemical stability are suitable for synthesis of new materials such as nano-particles, wires and networks of platinum and carbon within the pore system. In the case of the carbon synthesis, the fabrication technique has been fully developed so that ordered mesoporous carbons exhibiting Bragg X-ray diffraction (XRD) lines similar to those of the MCM-41-type mesoporous silica can be obtained after the complete removal of silica template.

### III-G-25 Study of the Growth of Boron Nanowires Synthesized by Laser Ablation

ZHANG, Yingjiu<sup>1</sup>; AGO, Hiroki<sup>1</sup>; YUMURA, Motoo<sup>1</sup>; OHSHIMA, Satoshi<sup>1</sup>; UCHIDA, Kunio<sup>1</sup>; KOMATSU, Toshiki<sup>1</sup>; IJIMA, Sumio<sup>1,2,3,4,5</sup>

(<sup>1</sup>AIST; <sup>2</sup>NEC; <sup>3</sup>JST; <sup>4</sup>Meijo Univ.; <sup>5</sup>IMS)

[*Chem. Phys. Lett.* **385**, 177–183 (2004)]

Boron nanowires with different morphologies and diameters have been fabricated by laser ablation. The effects of the synthesis temperatures, intensities of the laser beams, the types of the metal catalysts and the addition of H<sub>3</sub>BO<sub>3</sub> on the growth of the boron nanowires are studied. The systematic analyses show that the vapor-liquid-solid (VLS) model may play important roles in the growth of the boron nanowires.

### III-G-26 Structure and Electronic Properties of a Nongraphitic Disordered Carbon System and Its Heat-Treatment Effects

TAKAI, Kazuyuki<sup>1</sup>; OGA, Meigo<sup>1</sup>; SATO,

Hirohiko<sup>1</sup>; ENOKI, Toshiaki<sup>1</sup>; OHKI, Yoshimasa<sup>2</sup>; TAOMOTO, Akira<sup>2</sup>; SUENAGA, Kazutomo<sup>3</sup>; IJIMA, Sumio<sup>3,4,5,6</sup>

(<sup>1</sup>Tokyo Inst. Tech.; <sup>2</sup>Matsushita Indust. Co.; <sup>3</sup>AIST; <sup>4</sup>Meijo Univ.; <sup>5</sup>NEC; <sup>6</sup>IMS)

[*Phys. Rev. B* **67**, 214202 (11 pages) (2003)]

The heat-treatment effect on electronic properties is investigated in relation to structural change for pulsed-laser-deposited amorphous carbon thin films having  $sp^2/sp^3$  ratio  $\approx 9$ . The heat treatment at temperatures 200–400 °C increases conductivity and modifies the hopping conduction mechanism at low temperatures, resulting in the generation of a Coulomb gap at  $E_F$ . In the heat-treatment temperature region above 600 °C, considerably small positive thermoelectric power is suggestive of carrier compensation by the competition of hole and electron carriers that originate from the inhomogeneous charge. In the high-heat-treatment-temperature region 800–1100 °C, the formation of an infinite percolation path network of the graphitic  $sp^2$  domains induces an insulator-to-metal transition, where the electron transport in the  $sp^2$ -rich metallic state is featured by weakly temperature-dependent conductivity.

### III-G-27 Compression of Polyhedral Graphite up to 43 GPa and X-Ray Diffraction Study on Elasticity and Stability of the Graphite Phase

NAKAYAMA, Atsuko<sup>1</sup>; IJIMA, Sumio<sup>1,2,3,4,5</sup>; KOGA, Yoshinori<sup>1</sup>; SHIMIZU, Katsuya<sup>6</sup>; HIRAHARA, Kaori<sup>2</sup>; KOKAI, Fumio<sup>7</sup>

(<sup>1</sup>AIST; <sup>2</sup>Meijo Univ.; <sup>3</sup>NEC; <sup>4</sup>JST; <sup>5</sup>IMS; <sup>6</sup>Osaka Univ.; <sup>7</sup>Mie Univ.)

[*Appl. Phys. Lett.* **84**, 5112–5114 (2004)]

The crystal structure of polyhedral graphite particles (“G balls”) has been investigated under pressure up to 43 GPa and at room temperature by x-ray powder diffraction measurements. The polyhedra maintain the graphite phase under pressure higher than 40 GPa. A 29% compression in volume at 43 GPa involves an unusual decrease in the interlayer distance of 25%. The polyhedra recover their original crystal structure by releasing the pressure. A closed and solid structure of the polyhedra, suppressing a transition into another phase, causes them to become metallic under pressures higher than 20 GPa.

### III-H Spectroscopy and Photochemical Dynamics of the Methyl or the Methoxy Internal Rotation in Jet-Cooled Toluene Derivatives and Methylanisoles

The phenomena of energy relaxation in isolated molecules have been central in chemical kinetics over many decades. An extensive subject has been followed by the application of supersonic jet techniques, which enabled the study of well isolated ultra-cold molecules in jets. The jet-cooled molecules are isolated in gas phase, thus, the experiments are not subjected to interactions between molecules and solvents or to vibrational relaxation in condensed phases.

The large transition energy is reserved in optically electronic excited molecules where the idea of temperature for molecular internal energy is replaced by the excess energy, by which photodissociation is induced. Investigation of nonradiative electronic relaxation processes, *i.e.* internal conversion (IC) or intersystem crossing (ISC) between two electronic states of the same or different electron spin multiplicity of photoexcited molecules, respectively, has long been interest of the photochemical dynamics because of the important role of these processes in photochemical reaction system.

A triplet state serves as an important intermediate in nonradiative processes of excited molecules. The dynamics of the triplet state generation, *i.e.* ISC, plays an important role in photochemical processes. For instance, chlorinated benzene derivatives in the first excited singlet ( $S_1$ ) state have small values ( $10^{-2}$ ) of the fluorescence quantum yields, suggesting that the ISC process to excited triplet states takes place due to the large spin-orbit coupling induced by the heavy Cl atom effect. The excited triplet state molecules undergo the C–Cl dissociation whose quantum yield is almost unity. Accordingly, the investigation of the ISC process assists to understand the photochemical reactions.

The substituent of the  $\text{CH}_3$  or  $\text{OCH}_3$  group on the benzene ring should play an important role in their photoexcited states. When these molecules are excited to the singlet excited state, internal rotational bands of these groups are observed for lower frequency regions than  $200\text{ cm}^{-1}$  in the LIF excitation spectra. Measurements of these internal band intensities and their fluorescence lifetimes should give information on the relaxation dynamics of these molecules.

#### III-H-1 Conformational Isomerism and Excited State Dynamics of Fluoroanisole in a Supersonic Jet

ISOZAKI, Tasuku<sup>1</sup>; SAKEDA, Kosaku<sup>1</sup>; SUZUKI, Tadashi<sup>1</sup>; ICHIMURA, Teijiro<sup>2</sup>  
(<sup>1</sup>Tokyo Inst. Tech.; <sup>2</sup>IMS and Tokyo Inst. Tech.)

It is known that substituted phenol and anisole derivatives have some stable conformers of internal rotation around the  $\text{C}(sp^2)\text{--O}$  bond both in the ground and excited states. In many cases, their stable structures corresponding to the energy minimum are *planar* conformers such as the *cis* and *trans* conformers. But recently, in addition to the existence of most stable *planar* conformer, it is suggested that the second stable *non-planar* conformer should exist for *o*-substituted anisole derivatives. However, a little information on such a *non-planar* conformer is reported so far. It is expected that the electronic excitation of the *non-planar* conformer should induce the geometrical change of the methoxy group related to the benzene ring, and alter the excited state dynamics compared to the *planar* conformer.

From these points of view, it is interesting to investigate how halogenation on the benzene ring of anisole affects on the excited state dynamics. In this study on *o*-, *m*- and *p*-fluoroanisole, in order to clarify the electronic transitions of rotational isomers, substituent effect on conformational structure and vibronic structure, and differences of excited state dynamics between the rotational isomers, the LIF excitation and SVL dispersed fluorescence spectra were measured in a

supersonic jet. Figure 1 shows the LIF excitation spectra of *o*-, *m*- and *p*-fluoroanisole. The SVL dispersed fluorescence spectra were also measured by pumping each vibronic band observed in the LIF excitation spectra. The vibronic and vibrational bands observed in the spectra were assigned with the aid of quantum chemical calculations on the B3LYP/cc-pVTZ level. The SVL dispersed fluorescence spectra indicated that the vibronic mixing should take place in the  $S_1$  state, and the IVR process becomes more dominant with the higher excess energy.

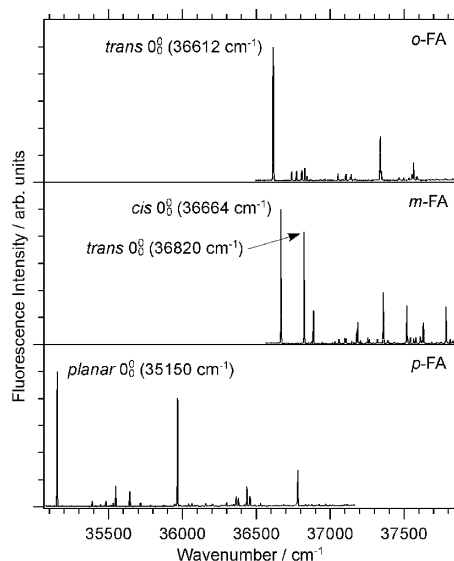


Figure 1. LIF excitation spectra of *o*-, *m*- and *p*-fluoroanisole.

### III-H-2 Spectroscopy and Relaxation Dynamics of Photoexcited Anisole and Anisole-Methyl-d<sub>3</sub> Molecules in a Supersonic Jet

MATSUMOTO, Ryu<sup>1</sup>; SUZUKI, Tadashi<sup>1</sup>; ICHIMURA, Teijiro<sup>2</sup>

(<sup>1</sup>Tokyo Inst. Tech.; <sup>2</sup>IMS and Tokyo Inst. Tech.)

In this work we measured the LIF and DF spectra of the  $S_1$ - $S_0$  electronic transition for jet-cooled anisole and anisole-methyl-d<sub>3</sub> molecules. This is the first time measurement of the fluorescence of the deuterated anisole species. The molecular orbital calculations on the molecular and vibrational structures on the electronic ground and excited state were also performed.

For anisole molecule, 3 vibrational modes in the  $S_0$  state and 11 vibrational modes in the  $S_1$  state were reassigned on the basis of experiments and calculations. For deuterated molecule, we assigned 13 and 12 vibrational modes in the  $S_0$  and  $S_1$  states, respectively. Dispersed fluorescence (DF) measurement clarified the anharmonic coupling between several vibrational modes. The Duschinsky rotation between the 10b and 16a, and 6a and 6b modes are significantly observed for

both molecules.

In order to investigate the relaxation dynamics we measured fluorescence lifetimes of the single vibrational levels for the first time and calculated the nonradiative decay rate constant. Among the nonradiative processes, intersystem crossing to the triplet manifolds would be dominant for both species, as in the case of the condensed phase. It was found that the character of the SVL is deeply related to the ISC process; the excess energy dependence of the  $k_{nr}$  becomes larger for the out-of-plane bands than for the in-plane bands. Especially the methyl internal rotation in the anisole molecule and vibrational mode of 16a in the anisole-methyl-d<sub>3</sub> molecule exhibited fast nonradiative decay process, revealing accepting modes of the ISC processes. The IVR process was affected by the methyl deuteration but the results were against the expectation; the broadening of DF spectra below 940 cm<sup>-1</sup> was depressed by deuteration. On the SVLs with in-plane component the broadening of DF spectra by the IVR and  $k_{nr}$  values are well correlated. Therefore we conclude the energy flow to the out-of-plane mode should be responsible for the nonradiative process.

## III-I Photophysics and Photochemistry of Aromatic Molecules in the Condensed Phase

Excited aromatic compounds generally release energy by various pathways such as photophysical processes and photochemical reactions. Electronically excited molecules are relaxed into a stable or metastable state through radiative and/or nonradiative processes as photophysical processes. It is well known that photochemical reactions occurring from excited state are bond dissociation, cyclization, isomerization, hydrogen abstraction, electron transfer, and so on. In addition, there exist relaxation processes and their quantum yields characteristic to each compound. It is very important to investigate photodynamics of excited molecules.

Intermediates such as excited states and radicals, which can be generated with laser irradiation, have been detected by laser flash photolysis as described. The shorter pulse width of a light source becomes, the shorter-lived intermediates can be detected. Furthermore, the properties of intermediates would be clarified. These informations should obtained photophysical and photochemical dynamics of the intermediate that are interested.

On the other hand, it becomes difficult to elucidate nonradiative processes, such as internal conversion and intersystem crossing from the excited state, by laser flash photolysis. Time-resolved photothermal techniques, however are powerful to study nonradiative processes because they can detect the released heat from excited molecules directly with high sensibility. They should be described in detail. Combination of photoexcited and photothermal methods will give us detailed information on photophysical and photochemical dynamics of intermediates, as well as excited states.

### III-I-1 Photochemical Dynamics of Phenoxy Alkanes

SUZUKI, Tadashi<sup>1</sup>; ANDO, Mayaka<sup>1</sup>; ICHIMURA, Teijiro<sup>2</sup>

(<sup>1</sup>Tokyo Inst. Tech.; <sup>2</sup>IMS and Tokyo Inst. Tech.)

Phenoxy radical is one of the fundamental chemical intermediates on the photochemistry. It is known to take an important role on combustion, lignin UV reaction in the plant, biochemical reactions, and so on. Photolysis of phenol and phenoxy alkanes is also known to produce phenoxy radical.<sup>1)</sup> In the gas phase phenoxy

methane (anisole, methoxy benzene) was reported to produce phenoxy radical with the 193 nm laser excitation.<sup>2)</sup> We measured transient absorption spectra of several phenoxy-substituted alkanes in solution, however, not only phenoxy radical but also another transient were found. In this study, we made an assignment of the transient and discussed the reaction dynamics in detail. Furthermore, reaction pathway for excited methoxy-substituted toluenes (*o*-, *m*-, *p*-methylanisoles) was also discussed.

The transient absorption spectrum of phenol in solution obtained with the UV irradiation shows a structured band at around 400 nm. It is known as a

typical absorption spectrum of phenoxy radical. However, the transient absorption spectrum of anisole was not the same spectrum of phenoxy radical; a broad absorption band appeared around 440 nm in addition to the structured band of phenoxy radical. The broad band was observed in the spectra of the polar and non-polar solutions. The lifetime of the transient was several  $\mu$ s. To make an assignment of the transient and to clarify the reaction mechanism, photosensitization experiment with acetone was carried out. The broad band appeared at around 440 nm, which is exactly the same one obtained with the photolysis of anisole. We could safely assign the new transient to a radical, which should be produced through hydrogen atom elimination by the UV irradiation.

#### References

- 1) G. Porter and F. J. Wright, *Trans. Faraday Soc.* **51**, 1469 (1955).
- 2) Y. Kajii, K. Obi, N. Nakashima and K. Yoshihara, *J. Chem. Phys.* **87**, 5059 (1987).

#### III-I-2 Relaxation Processes of Naphthalene in Highly Excited State in Condensed Phase

WATANABE, Sadayuki<sup>1</sup>; SUZUKI, Tadashi<sup>1</sup>; ICHIMURA, Teijiro<sup>2</sup>

(<sup>1</sup>Tokyo Inst. Tech.; <sup>2</sup>IMS and Tokyo Inst. Tech.)

Relaxation dynamics in highly excited singlet state of naphthalene (NP) in condensed phase is studied by time-resolved thermal lensing (TRTL) technique coupled with nanosecond laser photolysis. The results of TRTL measurements with the 248 nm excitation give heat conversion efficiency of NP, and lead to information on relaxation process, that is, rapid nonradiative process is found to take place from the highly excited singlet state ( $S_2$ ) into the  $S_0$  state, not through the  $S_1$  ( $v = 0$ ) state. The quantum yield is successfully estimated to be  $0.31 \pm 0.01$ . The occurrence of the rapid nonradiative process is also found in deuterated NP and 1-methylnaphthalene. The mechanism of the relaxation process from the highly excited state is discussed in detail.

#### III-I-3 Calorimetric Standards for Photothermal Methods at the 248 nm Excitation

WATANABE, Sadayuki<sup>1</sup>; SUZUKI, Tadashi<sup>1</sup>; ICHIMURA, Teijiro<sup>2</sup>

(<sup>1</sup>Tokyo Inst. Tech.; <sup>2</sup>IMS and Tokyo Inst. Tech.)

[*Chem. Phys. Lett.* **374**, 41–44 (2003)]

The time-resolved thermal lensing measurements were carried out on 2-hydroxybenzophenone, pyridazine and benzene in acetonitrile at the 248 nm excitation in order to investigate the feasibility for the calorimetric standards on photothermal methods. The heat conversion efficiency values of 2-hydroxybenzophenone and pyridazine were estimated to be unity compared with that of benzene, revealing that 2-hydroxybenzophenone and pyridazine should show no fluorescence and no photochemical reactions. Therefore, these molecules should be good calorimetric standards at the 248 nm excitation.

#### III-I-4 Production and Excited State Dynamics of Photo-Rearranged Isomer of Benzyl Chloride and Its Methyl Derivatives Studied by Transient Absorption and Time-Resolved Thermal Lensing Techniques

NAGANO, Mika<sup>1</sup>; SUZUKI, Tadashi<sup>1</sup>; ICHIMURA, Teijiro<sup>2</sup>; OKUTSU, Tetsuo<sup>3</sup>; HIRATSUKA, Hiroshi<sup>3</sup>; KAWAUCHI, Susumu<sup>1</sup>

(<sup>1</sup>Tokyo Inst. Tech.; <sup>2</sup>IMS and Tokyo Inst. Tech.; <sup>3</sup>Gunma Univ.)

[*J. Phys. Chem. A* submitted]

Production and photoexcited dynamics of reaction intermediates with photolyses of benzyl chloride (BzCl) and methyl-substituted benzyl chlorides (MeBzCl) were studied by using stepwise two-color laser excitation transient absorption (TC-TA) and two-color laser excitation time-resolved thermal lensing (TC-TRTL) measurements. With photoexcitation of BzCl the formation of transient photo-rearranged isomer was suggested in the previous paper [*Res. Chem. Intermed.* **27**, 137 (2001)]. Such an isomer formation for MeBzCl was also observed in a 248 nm excitation. It was found that further photoexcitation of the isomers with the 308 nm light caused photodissociation to yield the corresponding benzyl radicals. The reaction quantum yield and the molar absorptivity of the photo-rearranged isomer of BzCl were estimated. The heat of reaction for the photodissociation of the isomer was successfully determined with the TC-TRTL measurement. These experimental results were excellently consistent with ab initio and DFT calculations.

## III-J Excited State Dynamics of Organic Molecules in Cyclodextrin Nanocavities

### III-J-1 The Cavity Size Effect on the Excited State Dynamics of Dimethylaniline Derivatives Complexed with Cyclodextrins

MATSUSHITA, Yoshihisa<sup>1</sup>; SAKEDA, Kosaku<sup>1</sup>;  
SUZUKI, Tadashi<sup>1</sup>; ICHIMURA, Teijiro<sup>2</sup>  
(<sup>1</sup>Tokyo Inst. Tech.; <sup>2</sup>IMS and Tokyo Inst. Tech.)

[*Chem. Phys.* **286**, 399–407(2003)]

[*J. Phys. Chem. A* **108**, 7490–7495 (2004)]

The effect of cyclodextrin (CD) complexation on the excited state dynamics of some dimethylaniline derivatives, 4'-dimethylaminoacetophenone (DMAAP), methyl 4-(dimethylamino)benzoate (MDMAB), and ethyl 4-(dimethylamino)benzoate (EDMAB) in bulk solution was studied by means of steady state and time-resolved laser spectroscopy. The dimethylaniline derivatives complexed with CDs exhibited twisted intramolecular charge transfer (TICT) fluorescence whereas only the emission from the locally excited state was observed in aqueous solution without CD (Figure 1). In the case of  $\alpha$ -CD complexes of MDMAB and EDMAB, dual TICT emission from different microenvironments was observed. The dependence of TICT emission intensity on pH and  $\alpha$ -CD concentration suggested that the dual TICT emission can be attributed to the guest molecule in the 1:1 and 1:2 guest- $\alpha$ -CD complexes (Figure 2). Time-resolved emission spectra also indicate the formation of 1:2 complex with  $\alpha$ -CD and faster backward electron transfer from TICT state for 1:1 complexes.

Though the effect of CD complexation on TICT photochemistry has been interpreted in terms of the restriction on molecular motion and the reduced polarity effect introduced by CD cavities, these effects tend to have opposite effects on the TICT emission yield. Thus the overall effect of CD encapsulation is probably complicated and the problem is still in controversy. Our results indicate that polarity effect introduced by the hydrophobic cavity is the dominant factor in the controlling the photochemistry of dimethylaniline derivatives in CD complexes.

**Figure 1.** Dispersed emission spectra and emission decay profiles of MDMAB ( $2.5 \times 10^{-5}$  M) in aqueous solutions (a) without CD, and in the presence of (b)  $5.0 \times 10^{-4}$  and (c)  $5.0 \times 10^{-2}$  M of  $\alpha$ -CD excited at 315 nm.

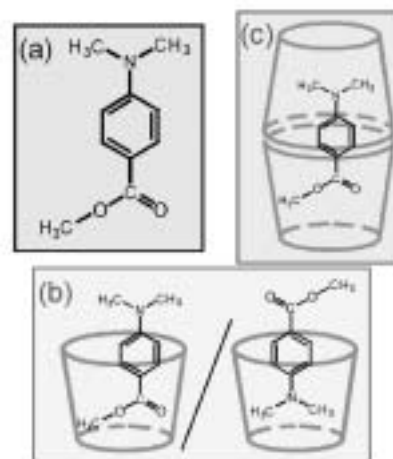
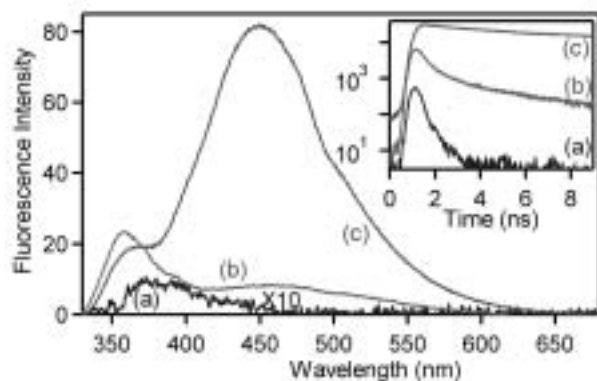


**Figure 2.** Possible structures of MDMAB- $\alpha$ -CD complex.



## III-K Wave Packet Engineering Using a Phase-Programmable Femtosecond Optical Source

We proposed “wave packet engineering” which realizes mutual conversion between phase information of photonic and quantum wave packets by means of light-matter interaction. A phase-programmable femtosecond optical source is indispensable for such interactive control of photonic and quantum wave packets. We demonstrate control of quantum wave packets in organic molecules and semiconductors using phase-programmed pulses.

### III-K-1 Molecular Phase-To-Amplitude Converter Using Femtosecond Wave Packet Engineering

MISAWA, Kazuhiko; MATSUDA, Isao<sup>1</sup>; LANG, Roy<sup>1</sup>

(<sup>1</sup>Tokyo Univ. Agric. Tech., CREST(JST))

[*Technical Digest of QELS04 IWA (2004)*]

The intensity of the spontaneous emission from a cyanine dye molecule (IR-140) is measured to evaluate the remaining excited-state population after photo-excitation with femtosecond chirped pulses. The chirped pulses are prepared by using the chirp variable device with a chirped mirror pair. The center wavelength, pulse energy, and duration of the output from the chirp device are 790 nm, 2 mJ, and 40 fs, respectively. The spectral profile does not change irrespective of the chirp condition. The ethanol solution of IR-140 at a concentration of  $2 \times 10^{-4}$  M is circulated in a 0.5-mm thick quartz cell. The fluorescence intensity is increased and decreased in case of positively chirped (PC) and negatively chirped (NC) excitations, respectively, with respect to the Fourier transform limited (TL) excitation. This chirp dependent fluorescence (CDF) results from the coherent interaction between the chirped pulses and the quantum wave packet in the material. The stimulated emission efficiency is different between the NC and PC excitation. At low excitation the stimulated emission is not efficient and CDF is negligible. As excitation is increased, CDF becomes remarkable. The intensity change is up to about 25 percent of the total intensity. To explain the dependence on the excitation intensity, we perform a quantum mechanical calculation based on a three-level model. Theoretically, an oscillatory dependence like Rabi oscillation is expected in case of NC excitation. However, such strong stimulated emission pumping is not experimentally remarkable. This is due to not only low excitation, but also dephasing in dye molecules.

### III-K-2 Wave Packet Engineering Using a Phase-Programmable Femtosecond Optical Source

MISAWA, Kazuhiko; MATSUDA, Isao<sup>1</sup>; HASHIMOTO, Naoyuki T.<sup>1</sup>; LANG, Roy<sup>1</sup>

(<sup>1</sup>Tokyo Univ. Agric. Tech., CREST(JST))

[*J. Mod. Opt.* in press]

A new optical telecommunication method combin-

ing time and frequency domain multiplexing is proposed by using phase-controlled femtosecond pulses. Each pulse in a pulse train can be used as data packet with data bits in the frequency domain. We name the new principle as “wave-packet engineering” to adjust amplitude and phase of the wave function in device materials arbitrarily by controlling spectral phase of femtosecond pulses. The optical phase-to-amplitude converter is demonstrated with organic dye molecules, in which the phase information in the phase-modulated pulses can be demodulated into the luminescence intensity. Luminescence intensity from cyanine dye molecules observed to be chirp dependent, and is explained quantum mechanically in terms of coherent population transfer. According the wave-packet engineering, a design principle of the device using semiconductor coupled quantum nanostructures is also discussed.

## III-L In-Situ Observation of Surface Reactions by Variable Temperature Scanning Tunneling Microscopy

Chemical reaction at a well-defined single crystal surface has been intensively investigated as a prototype for heterogeneous catalytic reaction, electrochemical reaction and corrosion. The surface chemical reactions are heterogeneous in nature reflecting the structural and electronic imperfections relevant to steps, vacancies and impurities. In addition, the surface reactions are significantly influenced by the presence of reactants and products which often form ordered arrays. Therefore, in order to get better understanding of the surface reactions, it is vital to unravel the nature of these local properties which are closely linked to chemical reactivity of the surfaces reactions. Advent of scanning tunneling microscopy (STM) has enabled us to tackle the challenge with the ability to image the surface reactions in both real-time and real-space with atomic resolution. We investigate the reactivity of novel one-dimensional (1D)  $-Ag-O-Ag-O-$  compounds formed upon the dissociative adsorption of oxygen molecule on Ag(110) by the use of variable temperature scanning tunneling microscopy (VT-STM). The 1D compounds are arranged periodically to form  $(n \times 1)-O$  ( $n = 2-7$ ) reconstructed structures in which their mutual distance changes in self-organized manner depending on the O coverage. In addition, 1D compounds show structural fluctuation in the low O coverage regime reflecting the low dimensionality. These intriguing characteristics make them promising as a model system to explore physical and chemical properties of nano-structured materials.

### III-L-1 In-Situ Observation of Chemical Reaction of the 1D Compounds with CO on Ag(110)

NAKAGOE, Osamu<sup>1</sup>; WATANABE, Kazuya<sup>2</sup>; MATSUMOTO, Yoshiyasu<sup>2</sup>; TAKAGI, Noriaki<sup>2</sup> (<sup>1</sup>GUAS; <sup>2</sup>IMS and GUAS)

The reduction of O adatoms of the 1D compounds with CO was investigated by using VT-STM. STM measurements were performed as titration measurements by first preparing the  $(6 \times 1)-O$  surface and then reacting O adatom with CO to form  $CO_2$  that desorbs immediately after the reaction at constant temperatures at 180–208 K. STM images of the same region were sequentially taken in the constant current mode using an electrochemically etched W tip under the CO pressure of  $3 \times 10^{-8}$  mbar. In order to reduce tip-surface interactions, a high tunneling resistance of  $> 1$  G $\Omega$  was used. From sequential images, it is found that the reactivity of O adatoms at the ends of 1D compounds is so high that the reaction occurs only at the ends. Reflecting the specific reactivity of O adatoms at the ends of 1D compounds, the O coverage is decreased linearly with the progress of the reaction. From the temperature dependence of the slopes of the titration curves together with the reaction model, the activation barrier was estimated to be 39.2 kJ/mol.

### III-L-2 Real-Time Observation of the Spatial Propagation of Reaction Front with Atomic Resolution: $H_2O + O \rightarrow 2OH$ on Ag(110) $(6 \times 1)-O$

NAKAGOE, Osamu<sup>1</sup>; WATANABE, Kazuya<sup>2</sup>; MATSUMOTO, Yoshiyasu<sup>2</sup>; TAKAGI, Noriaki<sup>2</sup> (<sup>1</sup>GUAS; <sup>2</sup>IMS and GUAS)

Interaction of  $H_2O$  with solid surfaces is important in broad spectrum of scientific fields ranging from meteorology to heterogeneous catalysis. The adsorption of  $H_2O$  on  $(n \times 1)-O$  has been studied extensively, and various adsorbed states are reported such as chemisorbed  $H_2O$ , multilayers,  $(OH)(H_2O)_n$ ,  $(OH)_2H_2O$  and

OH species. However, the reaction kinetics and the influence of these species on the kinetics are unknown. STM measurements were made for the structural variation occurring over the course of the reaction of O adatoms in the 1D compounds with  $H_2O$  at 175 K. While chemisorbed  $H_2O$  molecules and hydrogen-bonded  $H_2O$  clusters exist transiently at 175 K, formed OH species remain on the surface stably and form  $(OH)(H_2O)_n$  and  $(OH)_2H_2O$  clusters as a nucleation center. STM images of the same regions were sequentially acquired in the constant current mode using an electrochemically etched W tip under the  $H_2O$  pressure of  $1 \times 10^{-9}$  mbar. Sequential STM images revealed that the reaction is highly nonlinear such that the reaction proceeds explosively with propagating reaction front after an induction period. In the induction period the reaction occurs only at the ends of 1D compounds similar to the reaction with CO. The reaction front propagates on the surface like a tidal wave irrespective of surface steps and impurity islands with the velocity of 1 nm/sec. The reaction model is proposed that the formed OH species play a role of catalyst as follows: OH species act as a nucleation center to form  $H_2O$  clusters. Clustering of  $H_2O$  increases the local coverage of  $H_2O$  by extending the residence time and enhances the reactivity of  $H_2O$  located at the periphery of the cluster as a proton donor.